Wide-Range Autonomous Ingress Tactical Hunter (WRAITH) Final Design

Tri Phan[1], Nathaniel Hollman[2], Tiger Sievers[3] and Mohamed [4],
University of Kansas, Lawrence, Kansas, 66045, United States

I. Executive Summary

This report discusses the propulsion of the WRAITH missile using a turbojet, an updated version of the JASSM developed by Lockheed Martin. First, an operational range of speeds and altitudes were researched and postulated to develop the range of conditions the missile will experience. The missile was found to cruise at an altitude of 2,000-30,000 ft at Mach 0.71. The mission shows that the WRAITH is being launched from a high-speed, high-altitude fighter jet or a B-1 Lancer, but flight is at low altitude to avoid radar detection using terrain masking. A model of the atmosphere was developed, and the dynamic pressure ranges that WRAITH will experience were calculated. Additionally, the ideal turbojet analysis was conducted with a maximum turbine inlet temperature of 4000 °R and a practical compressor pressure ratio cap out at 10. The compressor analysis shows that the combination of two axial and a centrifugal compressor can achieve a maximum pressure ratio of 10. Performance calculations show that the engine thrust decreases with increasing altitude and Mach number, while specific impulse decreases as Mach number increases. Using the Breguet range equation with a lift-to-drag ratio of 3.93 and a fuel weight of 350 lbs. Finally, the analysis suggests that WRAITH has a maximum powered flight range of 360 miles, with a corresponding flight time of 11.4 minutes.

The performance analysis confirms that the propulsion system achieves a specific impulse ranging from 2,950 to 3,020 seconds at cruise conditions. Utilizing a fuel load of 350 lbs and a cruise lift-to-drag ratio of 3.93, the redesigned WRAITH demonstrates a maximum powered flight range of 360 miles (313 nm) and an endurance of 11.4 minutes. This results in a 40% range increase over the baseline design's 250 miles, successfully achieving the threshold requirement for the redesign effort. The total designed weight of the WRAITH is 1,975 lbs, with an aft CG of 77.21 inches.

[1] Responsible for Executive Summary, Propulsion.
[2] Responsible for Compressor Design.
[3] Responsible for Specific Impulse and Remaining Range.
[4] Responsible for Standard Atmosphere.

II. Background

The Wide-Range Autonomous Ingress Tactical Hunter (WRAITH) is a stealthy, precision-guided cruise weapon designed to be launched from stand-off ranges, fly at low observable altitude, with terrain following profile to penetrate enemy air defenses, and deliver a high-explosive warhead onto a fixed target with guided terminal homing. In this design we retain the Lockheed Martin JASSM's baseline mission and guidance suite but replace the conventional horizontal tail surfaces with a streamlined boattail rear fuselage and optimized aft control fins if needed. The boattail reduces radar and aerodynamic drag while shifting stability and trim requirements rearward. This configuration aims to preserve low observable characteristics and range while trading some longitudinal stability for improved cruise efficiency and simpler external signatures.

Table 1 The WRAITH Specifications

Baseline Design	Old Dimension	New Dimension
Body Diameter	21.61 in	21.61 in
Reference Area	369.25 in^2	369.25 in^2
Nose Length	40.68 in	40.68 in
Total Body Length	161.95 in	161.95 in
Elliptical Height	10.00 in	10.00 in
Elliptical Width	11.67 in	11.67 in
Roll Angles	0 deg	0 deg
Nose-tip Diameter	0 in	0 in
Center of Gravity Assumption	0.5 total length	0.5 total length
Effective Exhaust Area	23.76 in^2	23.76 in^2
Leading Edge Section Angles	0 deg	0 deg
Number of Surfaces	3	3
Sweep Angles	45 deg	45 deg
Wingspan	7.87 ft	9 ft
Root Chord Length	1.00 ft	1.00 ft
Nose Tip to Root Chord Leading Edge of Wing	60.6 in	60.6 in
Tail Area	0 ft^2	3.36 ft^2

Much of this geometry was found using a three-view of the JASSM rocket and using the total length as a base dimension [1]. The missile body was modeled in NX to measure the other derived geometry [2].

A. Mission Description

This report will observe these initial conditions and flight regime, specifically when discussing the dynamic pressure and Mach plots, as these conditions force the missile into vastly different circumstances. The WRAITH is launched at high altitude of 40,000 ft at Mach 0.9 from either a fighter jet or a B-1 Lancer. The theory behind this is that the aircraft is in supersonic flight and slows to Mach 0.9 to launch the WRAITH without forcing the missile into an unusual Mach range. The WRAITH then coasts down to 30,000 ft with its wings deployed to save fuel and increase

range and then begins powered flight while descending to 2,000 ft. The missile will aim to cruise at 2000 ft at 0.71 Mach to avoid radar detection to remain stealthy. When near the target, the WRAITH will decelerate a little to 0.6 Mach and will climb to 3,000 ft and will finally accelerate when descending to hit its target, reaching a speed of around Mach 0.9.

Operational Cruise Mach number: 0.71
Maximum Mach number: 0.9
Cruise altitude: 2000 ft – 30,000ft [3] and [4]
Operational AoA: less than 10 deg
Stall Effective AoA: 30 deg

III. Standard Atmosphere

The standard atmosphere was found using an online resource which provided the ratios of temperature, pressure, and density for increasing altitudes in kilometers [5]. A function was then created to interpolate this data, which was previously extracted to a .mat file for code efficiency. Atmospheric data was found for up to 80,000 feet in altitude, and the ratios of pressure, temperature, density, and the speed of sound are shown in Figure . Note that this data is the temperature states static values, or the stream values if observed at zero velocity.

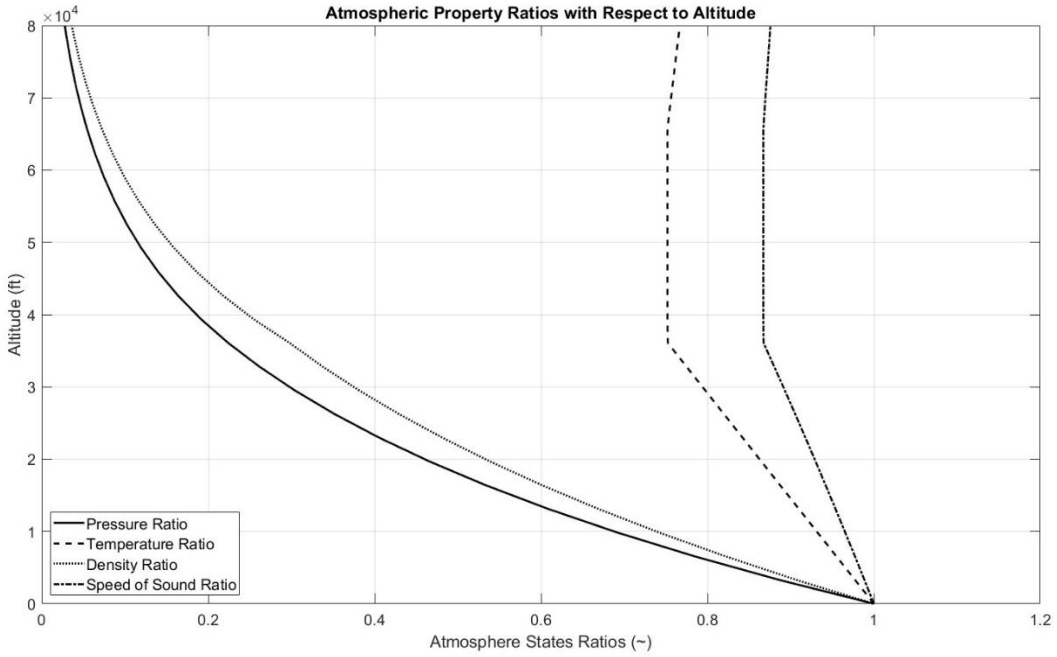

Figure 1 Standard Atmospheric State Ratios for 80,000 ft

These ratios are a multiplier of the local sea level absolute states. The standard sea level states were researched and found to be pressure = 14.7 psi, temperature = 518.7˚R, density = 0.002377 lb/ft^3, and the speed of sound = 1,117 ft/s. In general, pressure and density decrease with altitude and approach zero as they reach the boundary of space. Temperature decreases until around 40,000 ft, where it stays constant until around 65,000 ft where it starts increasing due to less protection from the sun. It was assumed for this that the gas constants did not change with altitude, so the

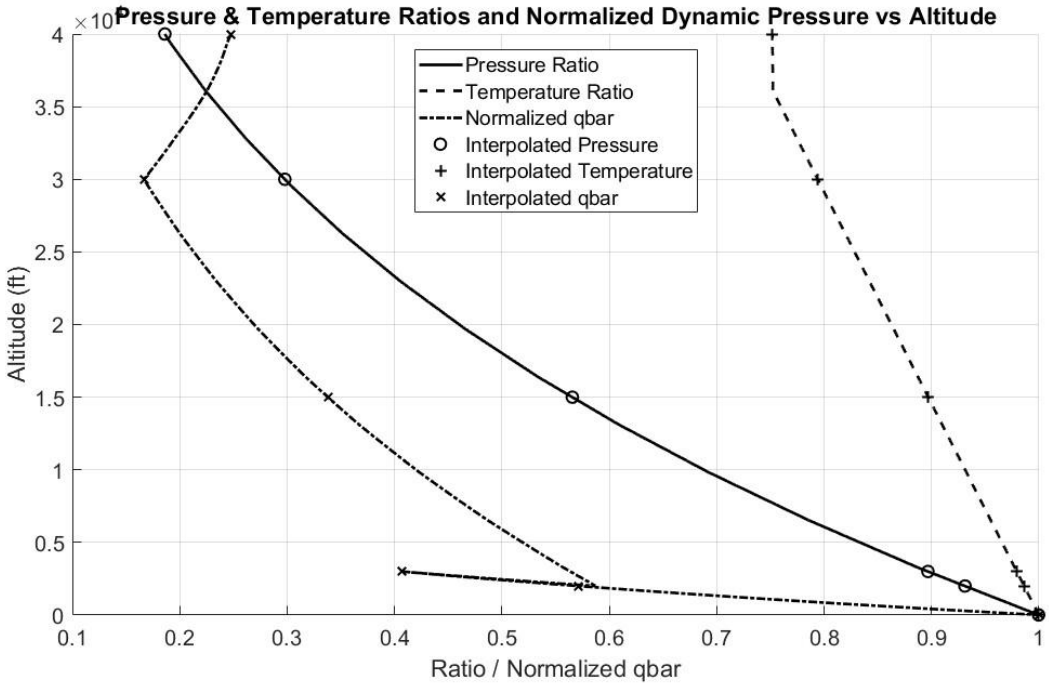

speed of sound ratio varied to the square root of the temperature. While this is an inaccurate assumption, for our true operational altitude, these values will minimally change, meaning that the assumption is not inaccurate for our operational ranges. With a defined ceiling of 40,000 ft, the plot of the states can be narrowed to the operational range in Figure 2.

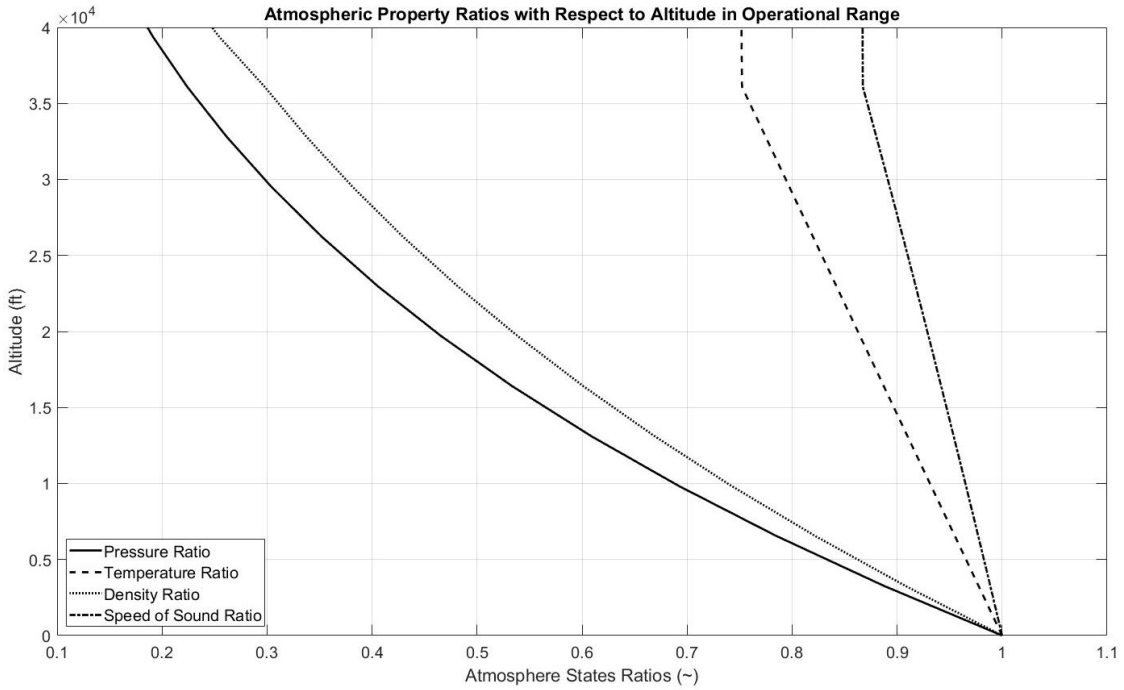

Figure 2 Standard Atmospheric State Ratios for Operational Range

The speed of sound ratio was then used to find the average Mach value for the operational range, which was found by averaging the ratio of the speed of sound and multiplying it by the ground speed of sound velocity. This yielded an average speed of sound of 1037 ft/s. The dynamic pressure can then be calculated for the operational range of Mach numbers using this average speed of sound and the change in density through altitude. The contours for these are shown for a range of Mach numbers in Figure .

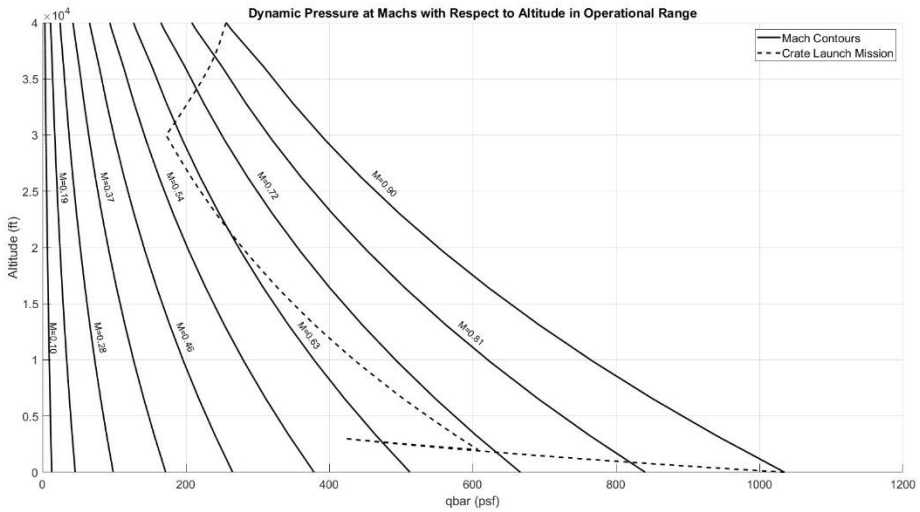

Figure 3 Dynamic Pressures at Various Mach Numbers and Altitudes

This plot also shows the two previously described missions flown in terms of altitude and dynamic pressure. Note that for different missions, the WRAITH must be within a dramatically different range of dynamic pressures as its altitude and Mach speed vary significantly. This shows how the controller for the WRAITH must consistently adapt to its current conditions, and the aircraft itself must be robust enough to fly at these varieties of conditions. As previously mentioned, in mission 1 the WRAITH is launched at slow speed at low altitude from a parachute-suspended crate and descends to the cruise altitude of 2,000 ft at Mach 0.71. Mission 2 is when the WRAITH is launched from a high altitude at a fast speed, such as from an F-22 at 40,000 ft, where it coasts to a lower speed, and then cruises to its point of Mach 7.1 at 2,000 ft. After this, it is estimated that on its descent to its target, it could reach a speed of Mach 0.9, so this is done to demonstrate the farthest extent of the dynamic pressure that the WRAITH could experience. This entire range describes how the WRAITH must be able to have a powerful enough control surface to maneuver at low dynamic pressures, while having an accurate enough surface to make minute adjustments at high dynamic pressures. Figure 4 combines the pressure and temperature ratios for the operational atmosphere, as well as the dynamic pressure normalized to the maximum dynamic pressure of 1034.9 psf.

Figure 4 Combined Atmosphere and Normalized Dynamic Pressure Plot

It is seen that the minimum dynamic pressure is at when the aircraft stops coasting to a lower altitude and begins the burn to its cruising altitude.

The ranges of the Mach numbers with their respective altitudes are then used to find the stagnation temperature of the free stream. Using the static temperature ratio from the standard atmosphere calculator shown with the plots above, the stagnation temperature can be found for the entire range of altitudes at each Mach number. Using the Mach number as a contour, Figure 5 can be found using Equation (1). The turbojet was only assumed to start burning at 30,000 feet, so an additional point was used in between the 30,000ft and 2,000ft segments.

$$T_{0t} = T_0\left(1 + \frac{\gamma_0 - 1}{2}M^2\right) \quad (1)$$

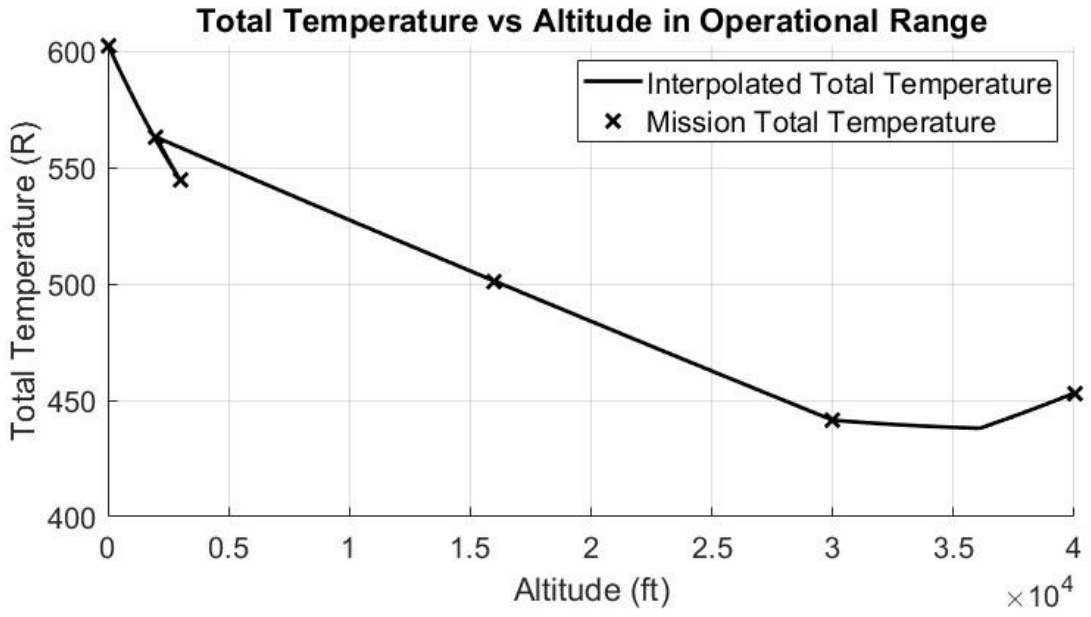

Figure 5 Varying Stagnation Temperature for Flight Regime

Using this plot, the range of stagnation temperatures can be found by finding the minimum and maximum stagnation temperature. This range was found to be from 441.5 °R to 602.7°R. Below is a table with the altitude, corresponding Mach number, and the Stagnation temperature for the range where the engine is on.

Altitude (ft)	30,000	15,000	2,000	3,000	10
Mach (~)	0.6	0.658	0.71	0.6	0.9
T_{0t} (°R)	441.5	505.6	563.1	544.6	602.7

IV.Weight

A. Structural Materials

The main structural material used for the structure of the WRAITH is high-grade carbon fiber. The example carbon fiber used is the M55J carbon fiber, with a high elastic modulus and high strength. While this material will cost more than other carbon fibers, this material was necessary to meet requirements for strength for the wing structure. Table 2 shows the properties of this material.

Table 2 Structural Material

Material	Elastic Modulus	Tensile Strength	Compressive Strength	Density
M55J Composite	49.31 Msi	291.53 ksi	127.63 ksi	0.069 lb/in^3

B. Warhead Weight

The warhead of a missile is the main determining factor of the weight of the missile, as heavier payloads require larger missiles. The warhead for the wraith will be kept the same as the JASSM warhead, which is a WDU-42/B penetrator. This 1000 lb warhead consists of a shaped charge ahead of the main warhead, which detonates to allow the main warhead to penetrate through shallow walls, and the main warhead which consists of 240 lbs AFX-757 and a steel fragmentation casing [3]. As the true design of this warhead is not publicly available, the warhead was modeled by making a cylindrical AFX-757 core surrounded by an even thickness of steel, with the core weight 240 lbs and the casing weighing 760 lbs. By setting the radius of the charge equal to 5 inches, the other geometric properties could be found using densities of 0.0650291 lb/in^3 for the explosive and 0.284 lb/in^3 for the steel casing. The found length of the explosive is 47 inches, and the thickness of the steel casing is 0.7335 in. Placement of the warhead in the missile is towards the front of the missile, while still leaving room for the front sensor. The decided placement was that the front of the warhead was 40 inches from the nose of the missile. As discussed later, this decision was made to move the center of gravity aft to reduce the static margin so that the missile is nimbler.

C. Fuel Weight

The weight of fuel placed in the missile is 350 lbs, which is the weight used to increase the range, as will be discussed later. The fuel tank is placed above the intake and turbojet of the missile. As the tank must be formed around these components, the geometry of the tank is very complex. The tank also cannot share a boundary with the fuselage skin as this would not allow the placement of important bulkheads throughout the entire missile. CAD was then used to design the fuel tank, and the location of where the tank began and ended is 88.5 in. and 144 in. from the nose respectively. Structure for the fuel tank was added by increasing the density of the volume in the CAD program, and so the total weight of the fuel tank was 361 lbs.

D. Engine Weight

The weight of the engine was derived from the JASSM missile engine, the Teledyne CAE J402. This engine weighs 101.5 lbs, and for simplification the turbojet weight for the WRAITH was estimated to be 100 lbs. An extra 31 lbs was added to this weight to account for any other components used to ensure that the engine functions properly, as well as any mechanical components for the vertical tails in the aft section of the fuselage. The engine was modeled using a simple cylinder in the aft section of the missile, beginning at 120 in. from the nose and ending at 145 in. from the nose. An exhaust was added to link the turbojet to the end of the missile. The material used is high strength steel and has the same thickness as the body, as will be discussed below. The weight of the outlet was found in NX to be 21.7 lbs.

E. Wing Weight

The weight of the wing is determined by the needed structure for the wing. The standard equation for thickness of a missile wing does not work in this case, due to the high span and aspect ratio of the wing. To then find the needed structure of the wing, the root moment of the wing must be found. The airfoil of the wing was estimated to have a total thickness of 1.1138 inches. The moment at the root of the wing was found by dividing the maximum lift by 2 and multiplying this by the distance from the center of one wing minus half the width of the fuselage. By then using the stress at the top and bottom of the root airfoil can be found. These are then used with the material allowables to find the maximum allowed lift of each wing. Equation (2) and (3) show how the root moment and stresses are found.

$$M = \frac{L_{max}}{2}\left(\frac{b_{wing}}{4} - b_{fus}\right) \tag{2}$$

$$\sigma = FOS\frac{M\frac{t_{airfoil}}{2}}{I} \tag{3}$$

It was found that to maximize the allowed lift, the 2nd moment of area should be maximized. To do this, the wing cross-section needed to be solid. This was then used as an approximation for the wing structure. Note that this is not completely accurate as there needs to be some hole to allow for a wire or pneumatic tube to go through the wing for the control surface. The wing structure also does not need to be solid all the way through, but this approximation will also account for any extra weight needed for the control surface structure and actuator. The 2nd moment of area for the wing was found using analysis in NX and was found to be 0.8274 in^4. Calculation of the maximum lift found that the total allowed lift of the wing was 13,793 lbs. For analysis of the fuselage structure, the wing weight of 106.2 lbs is applied where the wing is attached to the fuselage, which is from 57.3 in. to 69.3 in. from the fuselage nose.

F. V-Tail Weight

The weight of the V-tail was found through CAD analysis. The surfaces were approximated to be solid carbon fiber. This approximation accounts for any of the structural elements for how the fins fold inwards toward the fuselage, and how they are actuated for missile control. Each fin was found to weigh 13 lbs, and their weight location on the fuselage was found to be 136.7 in. to 150.8 in. from the fuselage nose.

G. Intake Weight

The weight of the intake was found by CAD analysis, using the same thickness as the skin. To make this change with different applied thicknesses, the volume was found as a function of surface area and thickness. The surface area of the intake was found to be 1762.8 in^2 so the volume and thus weight could be found by multiplying the area by thickness and then the density. The location of the inlet is from 61.73 in. to 120.1 in. from the fuselage nose.

H. Seeker and Avionics Weight

The weight of the seeker and avionics were estimated to be 40 lbs and 180 lbs respectively. These numbers were estimated simply from previous knowledge, as there are not many publicly available sources. Note that the avionics are heavy due to the needed resistance to jamming, meaning that the avionics may be in a Faraday cage to prevent external electromagnetic sources from disturbing the missile controller.

I. Fuselage Weight and Structural Analysis

The weight of the fuselage is determined by the surface area of the outer mold line and a determined thickness derived from the structural capabilities of the material. As there are many different stresses that the missile body must resist, the thickness is determined by many factors. To select a slightly conservative thickness, the squared average of the thickness given to each mode of failure will be used. The applicable modes of failure that will be observed are due to manufacturing, local bending buckling, local compressive buckling, local compressive stress due to thrust, and local bending stress due to the internal moment. First, the buckling allowables are found using Equations (4), (5), and the guessed thickness, then the thickness needed for manufacturing is found in Equation (6). The maximum stresses from bending and compression are found using Equations (7) and (8). Lastly, the thickness for each failure mode is then found using Equations (9), (10), (11), and (12). The total thickness required is found by multiplying the factor of safety by the square root of the sum of each thickness squared. Note also that internal pressure is not included as this thickness is only calculated for rockets, and any internal pressure will be contained by the jet engine or fuel tank.

$$F_{cr,b} = E * 0.35 * \frac{t_g}{a} \quad (4)$$

$$F_{cr,c} = E * 0.25 * \frac{t_g}{a} \quad (5)$$

$$t_{man} = 0.7d\left(\frac{p_{ext}}{E}\frac{l}{d}\right)^{0.4} \quad (6)$$

$$\sigma_c = T/(2\pi t_g r) \quad (7)$$

$$\sigma_b = M/(2\pi t_g r^2) \quad (8)$$

$$t_{cr,b} = 2.9r\sigma_b/E \quad (9)$$

$$t_{cr,c} = 4.0r\sigma_c/E \quad (10)$$

$$t_b = M/(2\pi F_{cr,b} r^2) \quad (11)$$

$$t_c = T/(2\pi F_{cr,c} r) \quad (12)$$

To find the maximum bending moment in the missile, a shear-moment diagram can be used. By setting the weights as distributed loads along the length of the fuselage, and adding the lift at the points that they are applied on the fuselage, the moment can be found by integrating the shear force, which is found by summing forces and balancing them. The maximum lift is found by taking the maximum possible lift generated by the body, then dividing the components of that lift by the maximum possible wing lift and multiplying them by the maximum allowed lift found I the wing weight section. By setting the location of the applied lift to where the body AC is, the location where the wing meets the body, and where the V-Tail connects to the body, the shear-moment diagrams can be made. The weight distribution and shear and moment diagrams are shown below in Figure 6. Note that the maximum shear is located where the lift is applied.

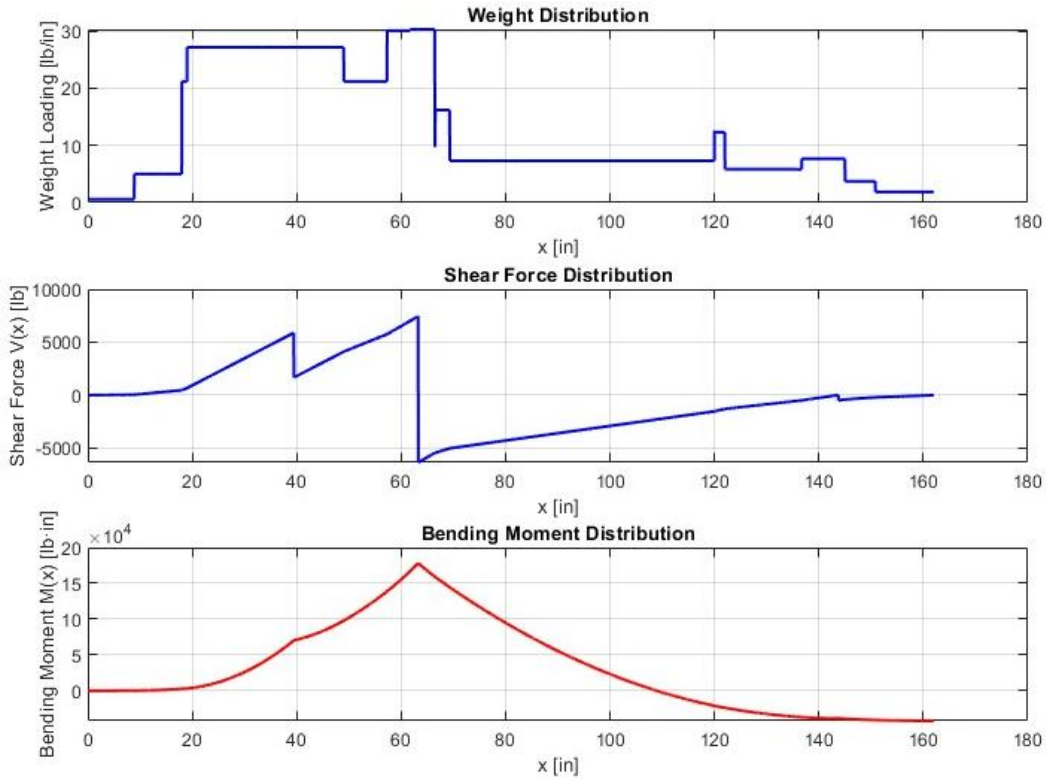

Figure 6 Weight, Shear, and Moment Diagrams

In the shear and moment diagram above, the weight is multiplied by the load factor, found by dividing the maximum allowed lift by the total weight. For this reason, the shear ends at zero. The reason the moment does not end at zero is since at this current lift configuration, the tail is not counteracting the pitching moment so the dynamic moment being applied is not zero.

By refining the guess thickness and recalculating, the skin thickness needed is around 0.1053 inches, so the thickness was made to be 0.11 inches. Using this, the weight of the fuselage was calculated to be 76.96 lbs. Bulkheads were added to increase strength. The thickness used for these bulkheads was twice the thickness of the skin. Eight bulkheads were added in total, and the sum of their weights was found using CAD to be 18.38 lbs.

J. Weight Summary

Table 3 below shows the summary of components and their weights. The total weight of the missile found from these components is 1975 lbs. This is significantly less than the JASSM missile weighs, which could be attributed to possible underestimations of weights, more modern materials, differing geometry, and limited access to substantiated documentation on the JASSM missile itself. This design is assumed to be the general first iteration of the WRAITH missile, so deeper design and analysis work into the subsystems of the missile would assuredly raise the weight of the missile to more realistic values. The center of gravity coordinates is in reference to the nose tip of the missile. These values were found in Siemens NX by modeling each component and assigning densities corresponding to the material or component weight.

Table 3 Component Weight Summary

Component	Weight (lb)	X_{cg} (in)	Z_{cg} (in)
Warhead	1000	64.25	0.00
Fuel Tank (full)	361	110.75	1.98
Engine	130.8	130.10	-1.40
Wing	106.2	79.30	9.42
V-Tail	26	147.89	4.85
Exhaust	21.7	148.73	-1.68
Inlet	13.4	98.55	-5.39
Seeker	40	15.95	-1.58
Avionics	180	36.5	-5.20
Fuselage Skin	77	79.30	-1.27
Bulkheads	18.38	67.89	-1.43

Figure 7 below visually shows where these components have been placed as well as the general layout of the missile.

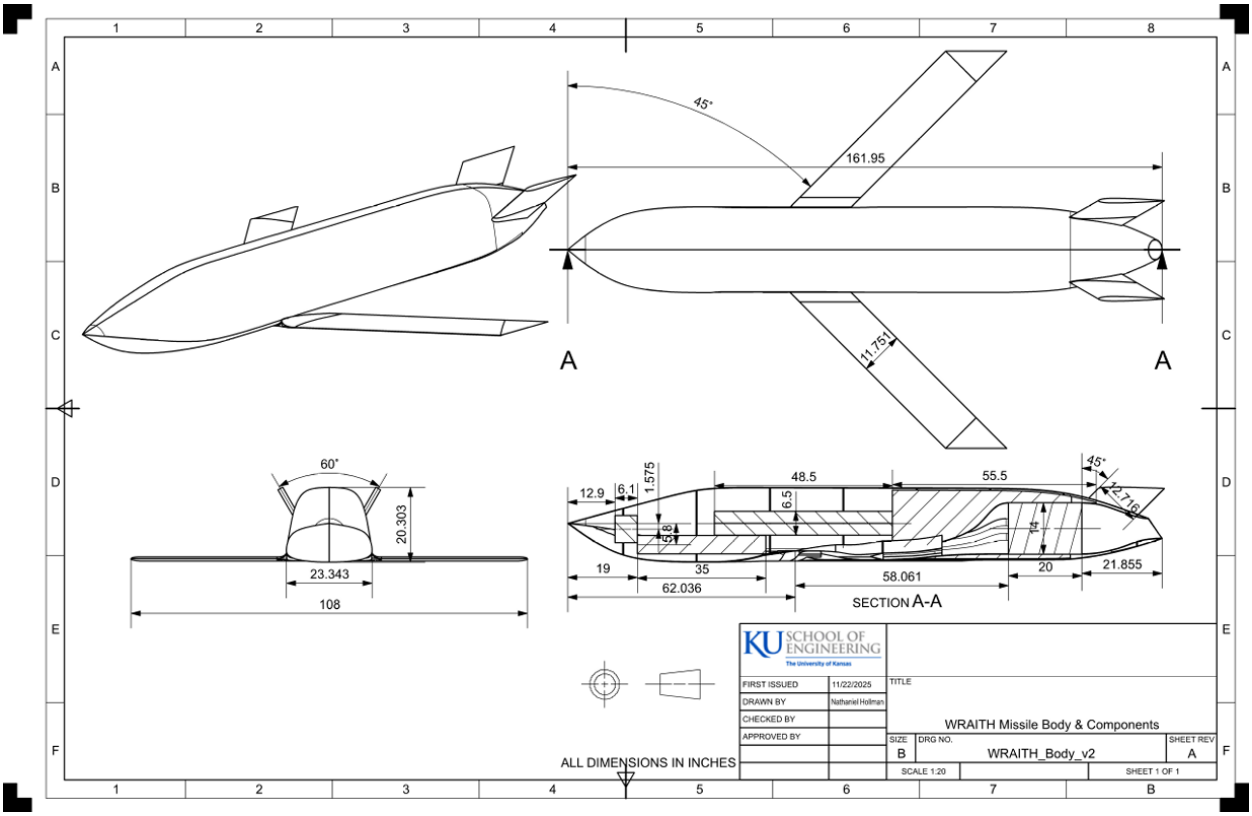

Figure 7 WRAITH Engineering Draft

As fuel is used while the missile travels, the weight characteristics change. Since the fuel tank is positioned aft of the center of gravity, as the fuel empties the center of gravity moves forward. Also, since the weight is decreasing, the moment of inertia of the missile moves forward. Table 4 shows this change in center of gravity and moment of inertia, where the center of gravity coordinates are in reference to the nose tip of the missile.

Table 4 Fuel Weight Change Summary

Fuel Weight (lb)	Total Weight (lb)	X_{cg} (in)	Z_{cg} (in)	I_{yy} (slugft^2)
350	1975	77.21	-1.16	17,997
262.5	1887	75.66	-1.23	16,965
175	1800	73.95	-1.30	15,932
87.5	1712	72.07	-1.37	14,900
0	1625	69.97	-1.44	13,868

As seen in the table, the center of gravity ranges from 77.21 inches with full fuel to 69.97 inches from the nose tip. These changes are plotted in Figure 8. It was also found that in the folded configuration, the center of gravity was 77.61 inches from the nose, which makes sense as the major change is that the wings fold backwards, moving the net mass backwards.

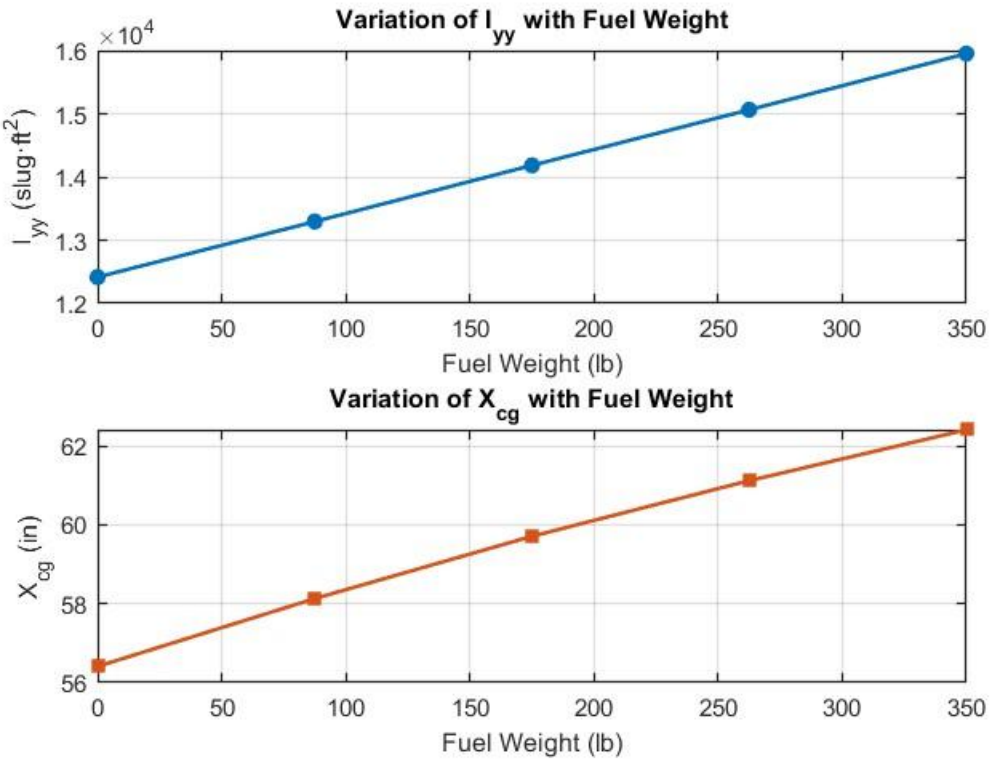

Figure 8 CG and Moment of Inertia Changes

The above figure shows that the change in moment of inertia for fuel depletion is very linear, while the CG change is mostly linear, with a small inward curve. The relationships both can assumed to be mostly linear relationships for simulation purposes, as the curvature of the CG plot is very small relative to the scale of the plot.

V. Aerodynamics

K. Total Mean Aerodynamic Center

The mean aerodynamic center for the WRAITH was determined using the following equation,

$$x_{ac,total} = \frac{C_{N_\alpha,b}\, x_{ac,b} + C_{N_\alpha,w,eff} x_{ac,w} + C_{N_\alpha,t,eff} x_{ac,t}}{C_{N_\alpha,total}}$$

Which sums up the contributions to lift from each of the lifting components and the individual aerodynamic center to find the total aerodynamic center. The resulting aerodynamic center for the missile at cruise is shown in 9.

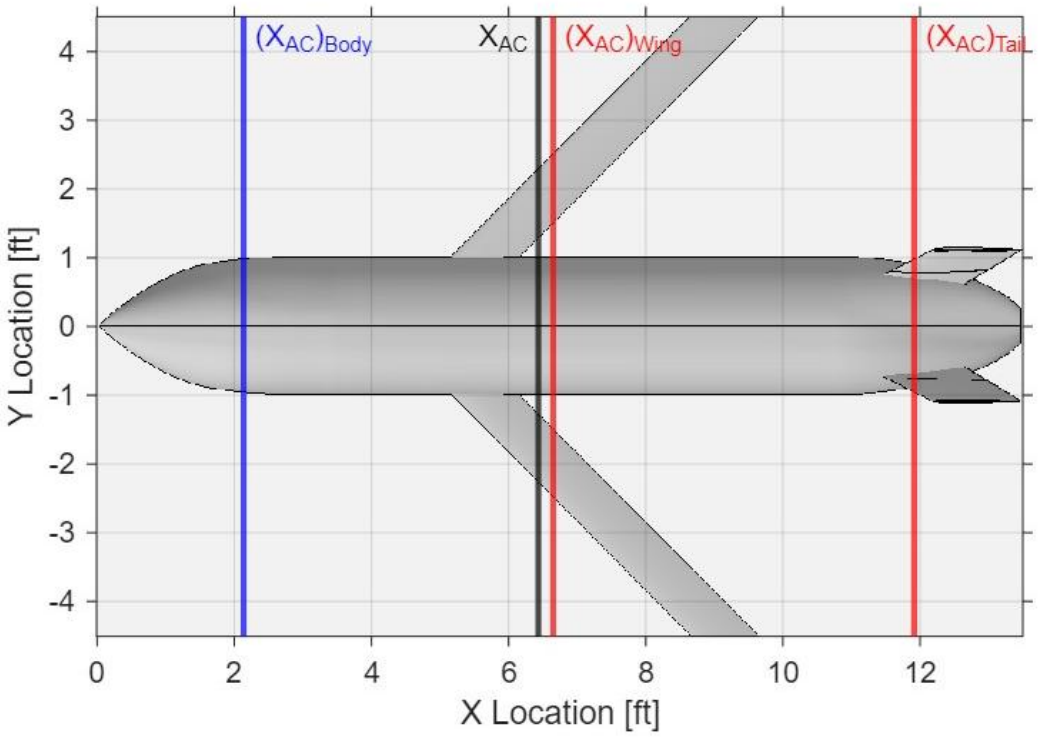

Figure 9 Mean Aerodynamic Center at Cruise Conditions

The aerodynamic center of the body is then found for all the angles of attack in the range from 0 to 30 degrees, and this is shown in Figure 10.

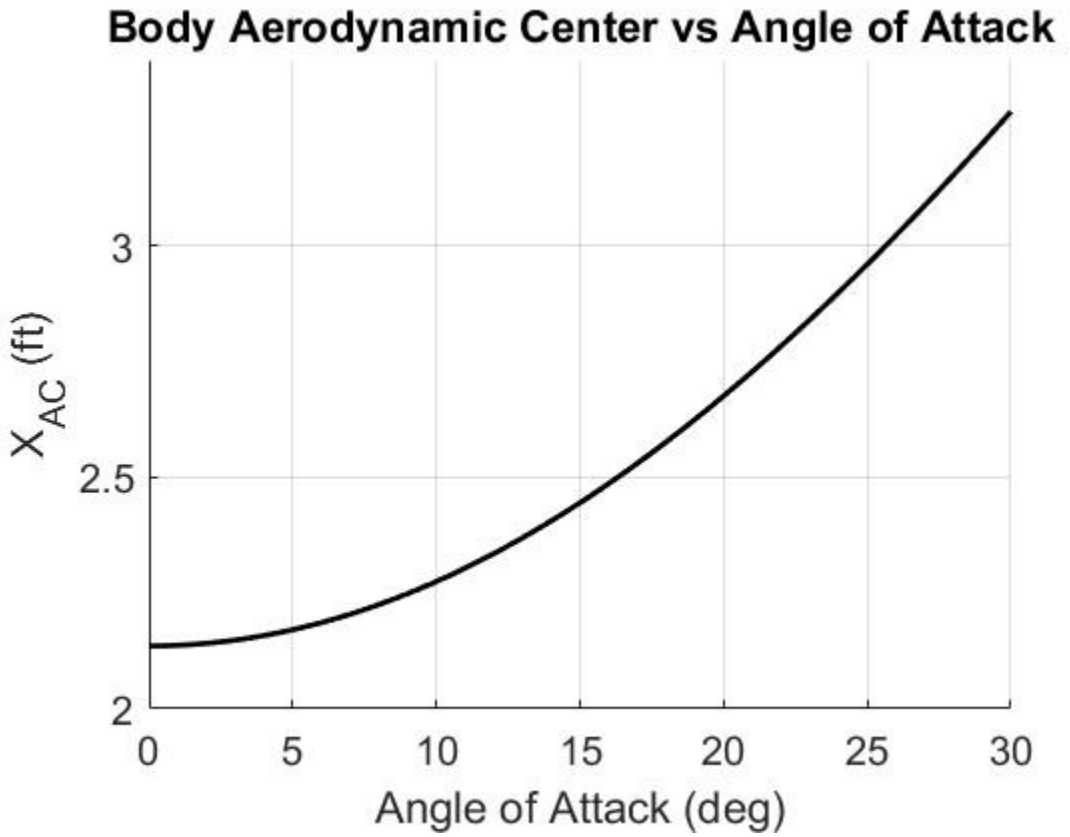

Figure 10 Body Aerodynamic Center per AoA

Increasing the angle of attack results in a rearward shift of the aerodynamic center. This is impacted largely by the shift in the body aerodynamic center, characterized by the body aerodynamic center equation. The aerodynamic center of the body is highly dependent on the angle of attack. This is clearly shown in figure 10, with the body aerodynamic center showing a noticeable shift from 1 to 30 degrees. Planar surfaces show minimal shift in the aerodynamic center. Below Mach 0.7, the aerodynamic center is assumed to be $0.25\bar{c}$. This is illustrated in figure 11, with the wing and tail showing no shift due to angle of attack.

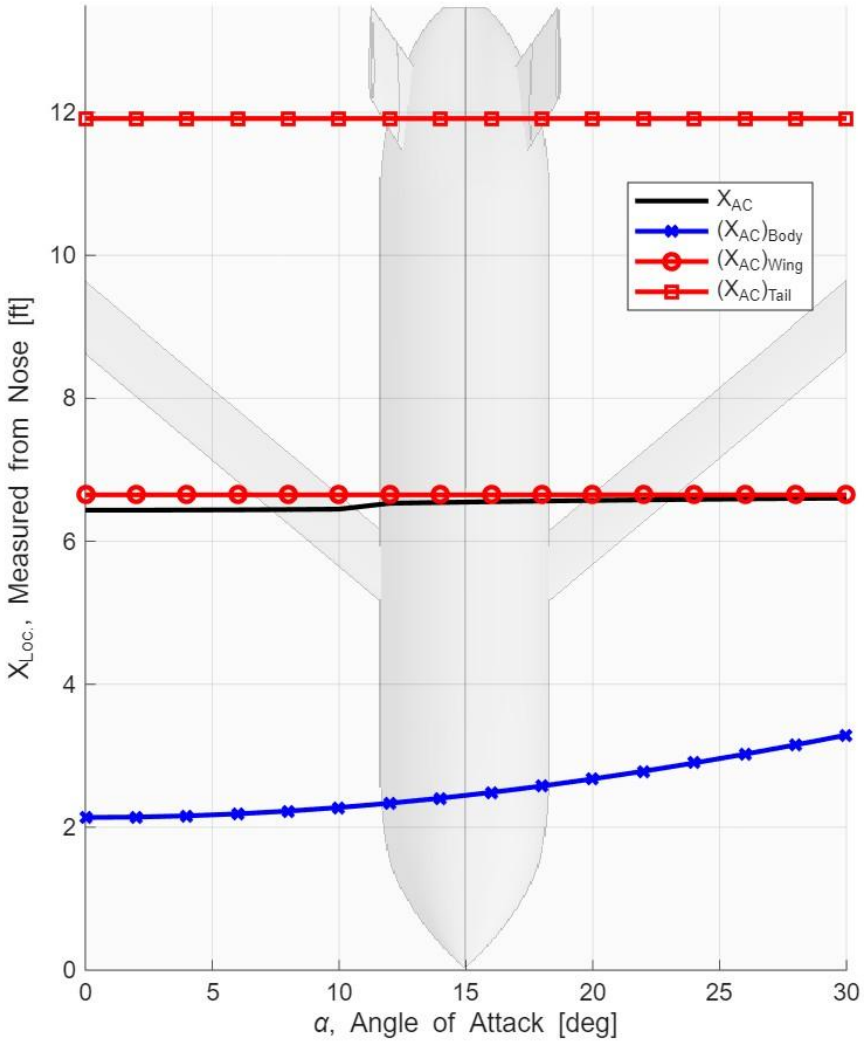

Figure 11 Aerodynamic Center Shift due to Angle of Attack

Overall, the aerodynamic center of the missile is dominated by the large wing, with the body and tail having minor contributions overall. The jump in aerodynamic center at 10 degrees is due to the discontinuity in the equations used for planar normal forces at high and low angles of attack. This increases the contribution of the wing and tail, in turn causing the increase in the aerodynamic shift. The equations describing this behavior are shown below.

Wing

$$C_{N_\alpha} = \frac{2\pi\,\mathrm{AR}}{2 + \sqrt{\mathrm{AR}^2(1 + \tan^2\Lambda_{\mathrm{LE}}) - M^2 + 4}} \qquad \text{for } \alpha' < 10^\circ$$

$$C_N = \left[\frac{2\pi\,\mathrm{AR}}{2 + \sqrt{\mathrm{AR}^2(1 + \tan^2\Lambda_{\mathrm{LE}}) - M^2 + 4}}|\sin\alpha'\cos\alpha'| + 2\sin^2\alpha'\right]\left(\frac{S_{\mathrm{surf}}}{S_{\mathrm{ref}}}\right) \quad \text{for } \alpha' > 10^\circ$$

Tail

$$C_{N_\alpha} = \frac{\pi A_T}{2} \qquad \text{for } \alpha' < 10^\circ$$

$$C_N = \left[\left(\frac{\pi\,\mathrm{AR}}{2}\right)|\sin\alpha'\cos\alpha'| + 2\sin^2\alpha'\right]\left(\frac{S_{\mathrm{surf}}}{S_{\mathrm{ref}}}\right) \qquad \text{for } \alpha' > 10^\circ$$

L. Tail sizing

The original WRAITH tail was designed to be a V-tail with the following dimensions:

- Span: $b_{T,old} = 2.40$ ft
- Root chord: $c_{r,T} = 1.50$ ft
- Tip chord: $c_{t,T} = 1.30$ ft

The Tail Area was calculated using the following equation and founded to be 3.36 ft^2.

$$S_T, old = b_T, old\,.\frac{C_{rT} + C_{tT}}{2}$$

The new WRAITH CG point is 77.21 inch from the nose of the missile which resulted in a negative static margin at cruise conditions (M = 0.71, h = 2000ft). To get static margin of zero new tail size was considered. The analysis showed that slightly smaller tail area than the original was needed to get static margin of zero as shown in graph 12.

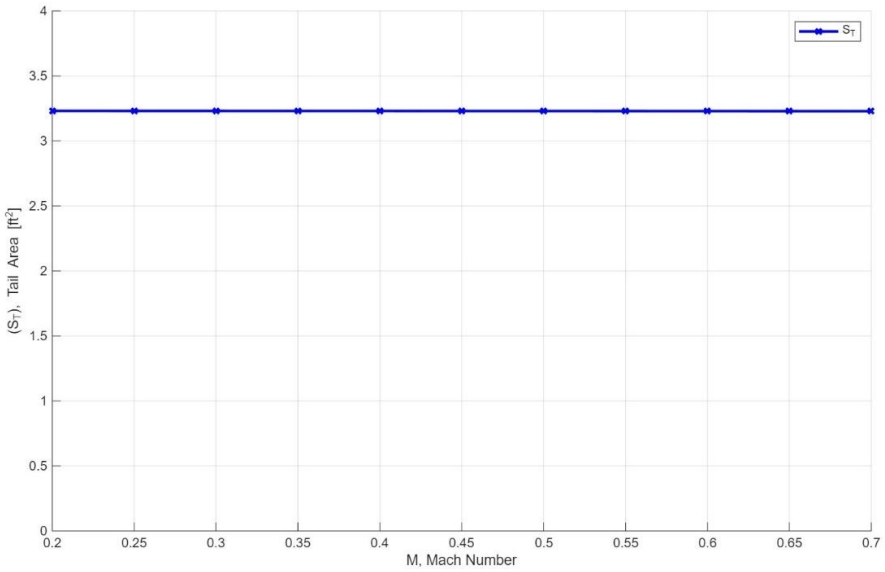

Figure 12 Required Tail Area for SM = 0 at Cruise

To get required tail area to set SM to zero at cruise the tail span was reduced while keeping same root and tip chords.

- Span: $b_{T,old} = 2.31$ ft
- Root chord: $c_{r,T} = 1.50$ ft
- Tip chord: $c_{t,T} = 1.30$ ft

Which resulted to a new tail area of 3.23 resulting in SM = 0.

M.Drag Analysis

The drag performance of the redesigned WRAITH missile was evaluated using MATLAB across the operational Mach range. Zero-lift drag coefficients were calculated separately for the body, wing, and tail using aerodynamic geometry inputs and the friction estimation method based on the Atmosphere and Planar Friction functions. Both powered and coasting conditions were considered. For powered flight, the engine exhaust induces additional base drag, while coast condition represents free-flight behavior without thrust contribution.

The total drag coefficient was then computed by summing the individual component values according to:

$CD = CD_0,body + CD_0,wing + CD_0,tail$

Body

To calculate the body drag with the boattail as a drag reduction method the following equation was created:

$$(C_{D_0})_{base} = \left(\frac{A_B - A_E}{S_{ref}}\right)(0.12 + 0.13 * M^2)$$

$$(C_{D_0})_{base} = \left(\frac{A_B}{S_{ref}}\right)(0.12 + 0.13 * M^2)$$

Since that the WRAITH only flies in the subsonic range only friction drag need to be calculated using the following formula :

$$(C_{D_0})_{Body,Friction} = 0.053\left(\frac{l}{d}\right)\left(\frac{M}{ql}\right)^{0.2}$$

Using these equations, the following plots are found for the total drag for coast and powered flight and are shown for the Mach range in Figure 13 and the components of drag for coasting flight are shown for the Mach range in Figure 14.

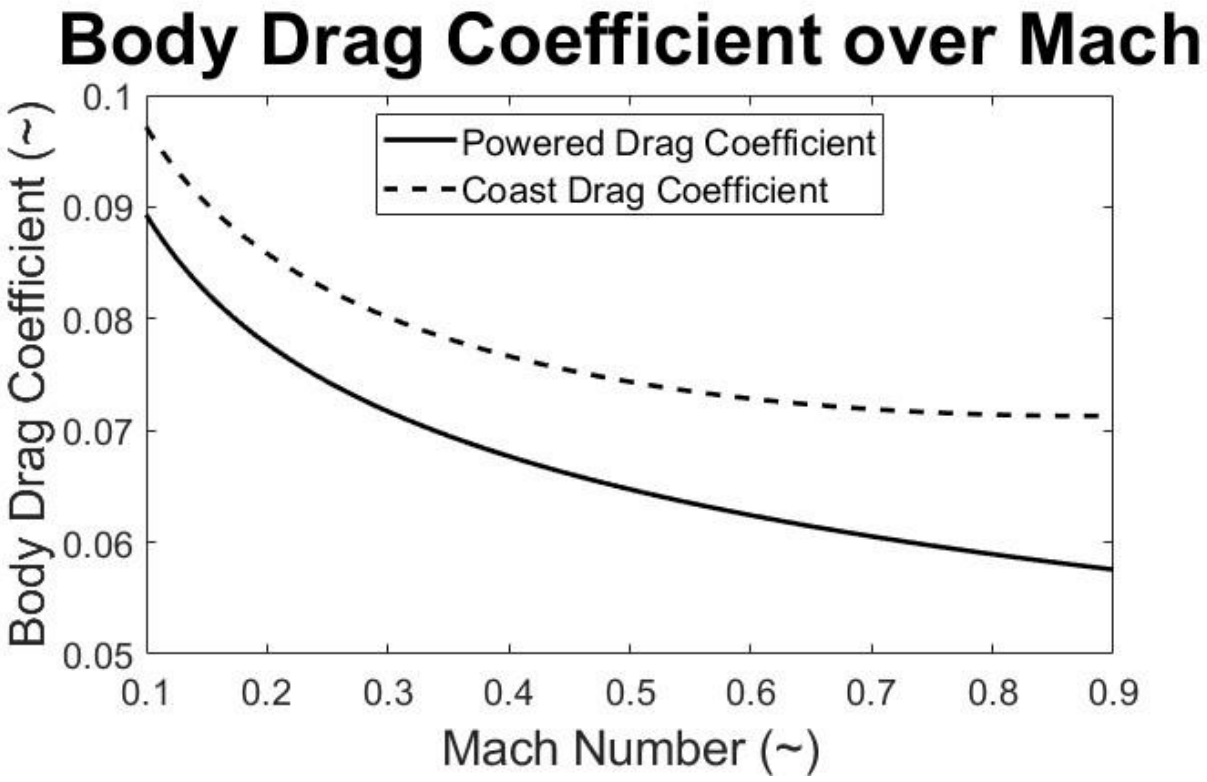

Figure 13 Body Drag per Mach Number

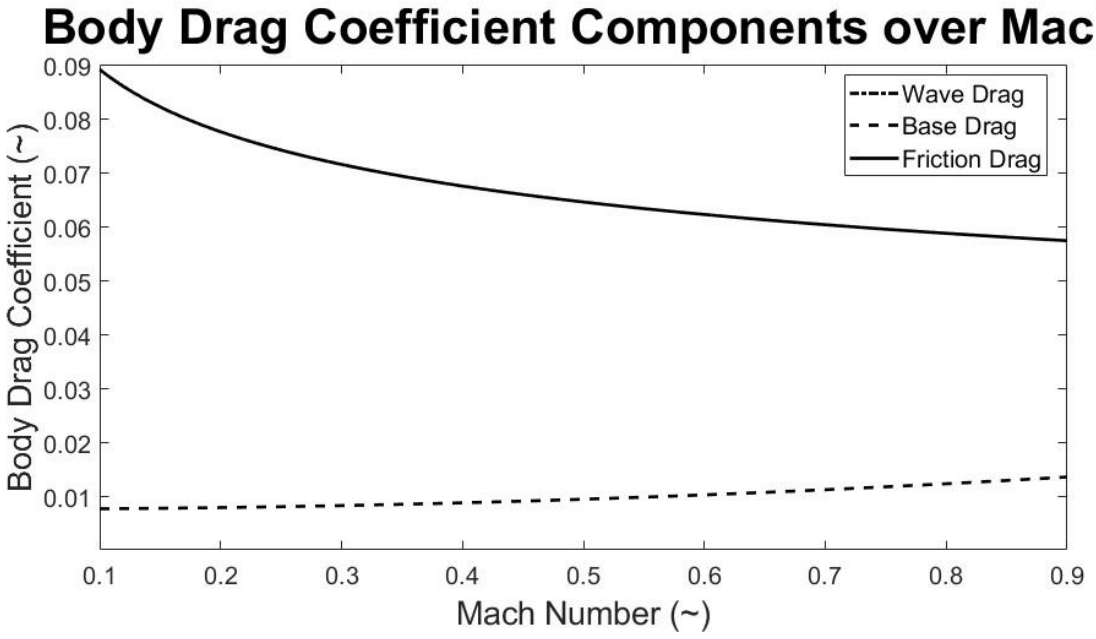

Figure 14 Coast Body Drag Components

Wing

For the wing the drag was calculated using the following formula:

$$C_{D0,wing} = \left(\frac{0.455}{[\log_{10}(Re)]^{2.58}(1 = 0.144M^2)^{0.65}}\right).\left(\frac{S_{wet,wing}}{S_{ref}}\right).n_w$$

Calculated drag coefficient for wing is shown in graph 15.

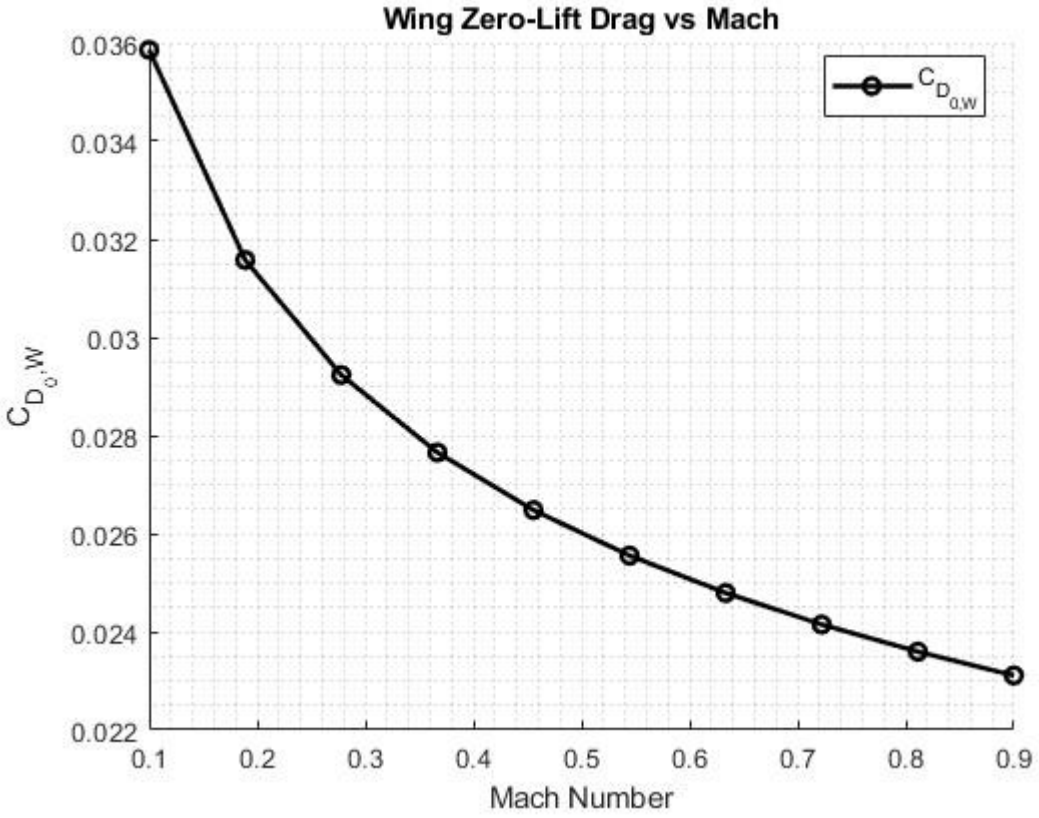

Figure 15 Wing Drag Vs. Mach

Figure 15 shows how the wing's zero-lift drag decreases significantly with increasing Mach, as expected for a swept lifting surface operating under compressibility effects. This trend helped reduce total drag in cruise conditions and improved lift-to-drag performance.

Tail

To get a zero static margin the tail was resized from a area of 2.40 $ft^2$to 2.31 ft^2. Using the planform friction equation described previously, Figure 16 was produced, showing the drag contribution of the tail over the flight envelope.

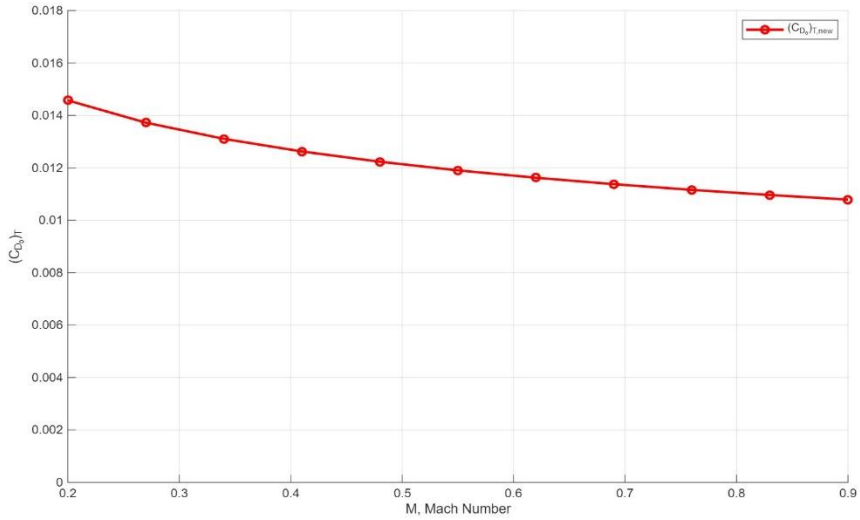

Figure 16 Tail Drag

The figure clearly shows that the drag produced from the tail is relatively small and considered worth it with the cost of additional controllability and maneuverability it adds.

Total Drag

The total drag coefficient of the WRAITH is found by summing the drag coefficients from each component. Figure 17 shows these contributions over the changing Mach number.

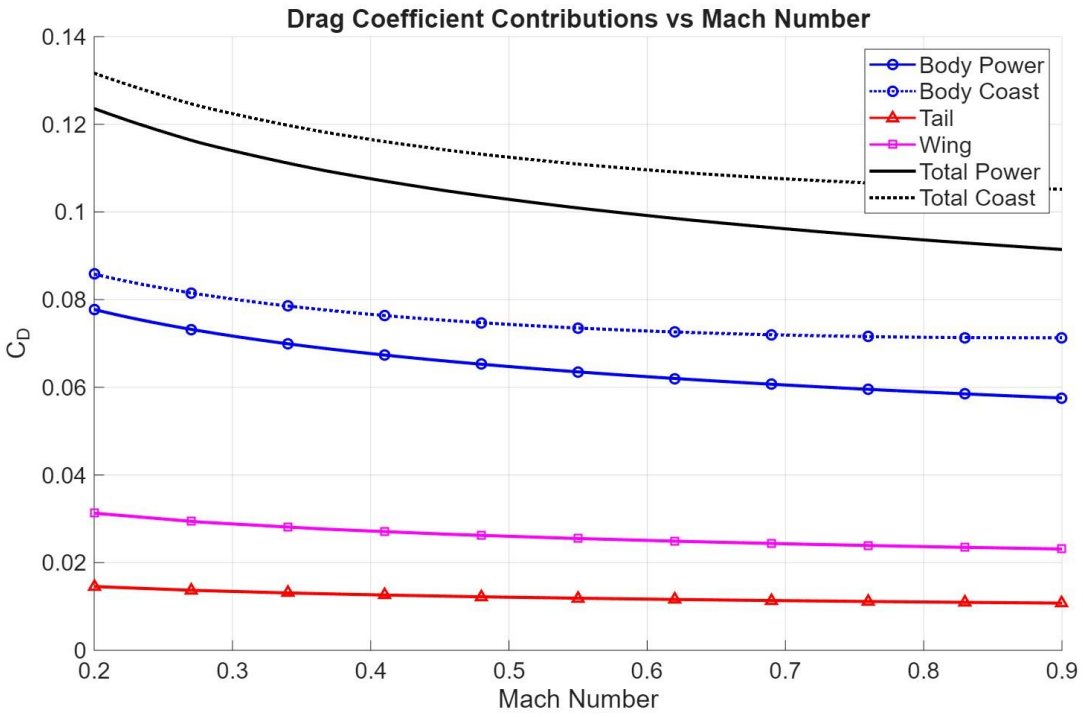

Figure 17 Drag Coefficient vs Mach Number

As shown in figure 17 the body exhibits the highest drag contribution due to its shape, followed by the wing and then the tail. The powered condition remains consistently higher than coasting across the Mach range due to the presence of exhaust effects.

N. Lift Analysis

The normal force produced by the body is a function of the angle of attack, roll angle, and approximated elliptical body geometry. Below is the equation for body normal force for a range of angles of attack and roll angles.

Body

$$C_{N_{Body}} = \left(\frac{a}{b}\cos^2(\phi) + \frac{b}{a}\sin^2(\phi)\right)\left(\left|\sin(2\alpha)\cos\left(\frac{\alpha}{2}\right)\right| + 1.3\frac{l}{d}\sin^2(\alpha)\right)$$

Using this equation for the range of angles of attack and roll angles, the plot for this is shown in Figure 18.

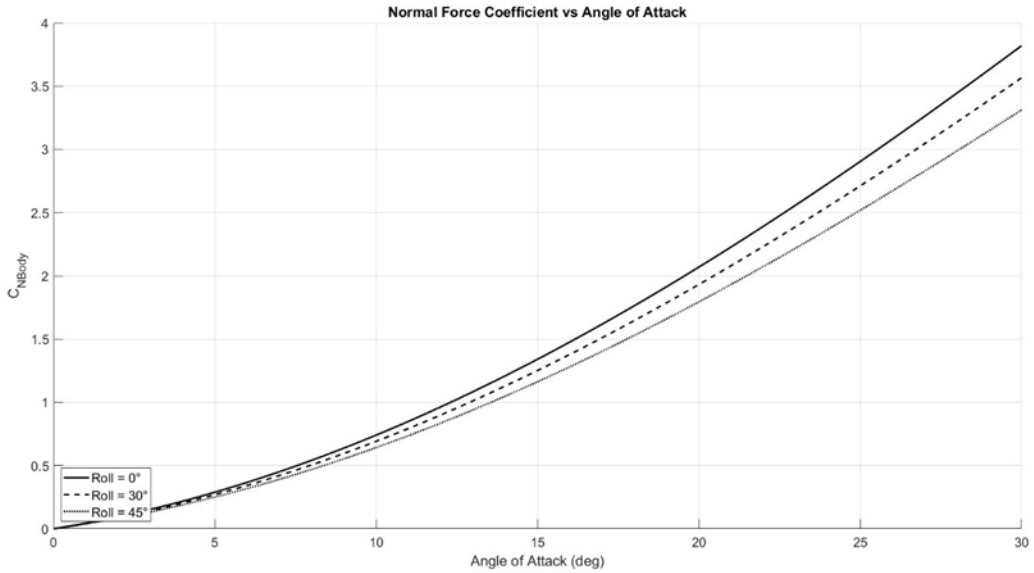

Figure 18 Body Normal Coefficient Range

It is observed that as expected, the angle of attack has a direct relationship with the normal force, and it is almost linear. Note also that since there is less cross-sectional area on the side of the missile, as it rolls it loses body lift.

Wing

For the wing, the analysis was extended to α=30 degrees to study near-stall behavior. Figure 19 shows the normal force produced by the wing over different Mach numbers.

$$(C_{N_\alpha})_{\text{surface}} = \frac{dC_N}{d\alpha} \approx \frac{dC_L}{d\alpha} = \frac{2\pi A}{2 + \sqrt{A^2\left(1 + \tan^2 \Lambda_{LE}\right) - M^2 + 4}} \quad [\text{rad}^{-1}]$$

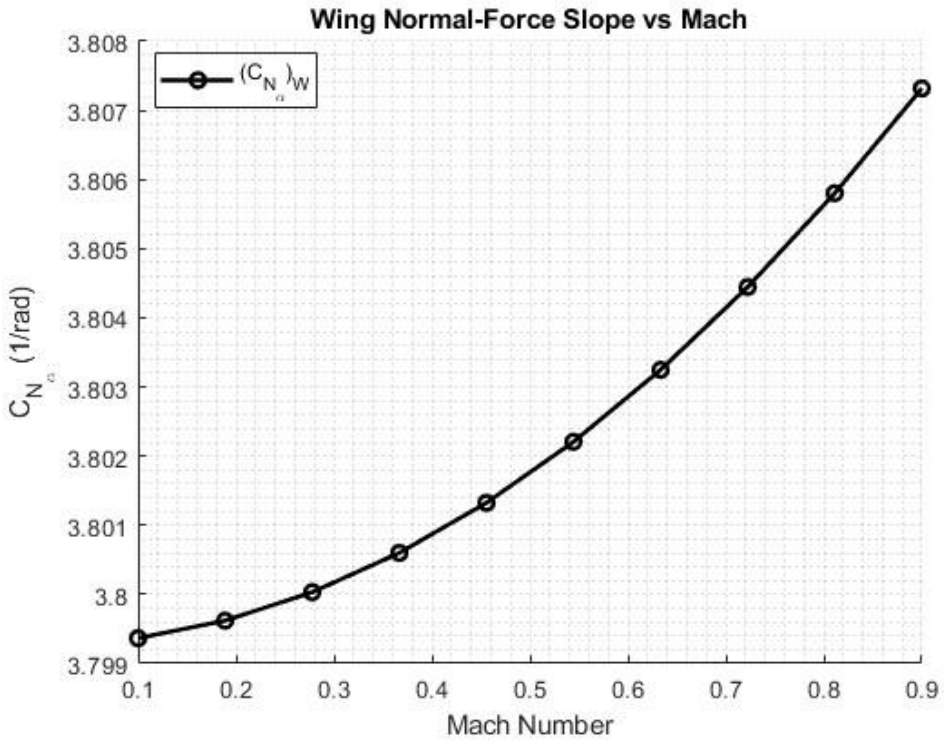

Figure 19 Normal Force Slope Vs. Mach

the wing's normal-force was modeled across both low and high angles of attack. The wingspan is 9 ft, so the missile has high lift efficiency while maintaining low drag. To capture behavior near the stall, the analysis range for angle of attack was extended from 10° to 30°.

For small angles ($\alpha < 10$), the flow remains attached and follows the linear relation:

$$C_{N,W} = (C_{N\alpha})W\alpha$$

At higher angles ($\alpha > 10$) where partial flow separation occurs; the nonlinear effect is modeled using the following equation:

$$C_N = \left[\frac{2\pi\,\text{AR}}{2 + \sqrt{\text{AR}^2(1 + \tan^2 \Lambda_{\text{LE}}) - M^2 + 4}} |\sin\alpha' \cos\alpha'| + 2\sin^2\alpha'\right]\left(\frac{S_{\text{surf}}}{S_{\text{ref}}}\right) \quad \text{for } \alpha' > 10°$$

Figure 20 shows the change in normal force coefficient for different angles of attack.

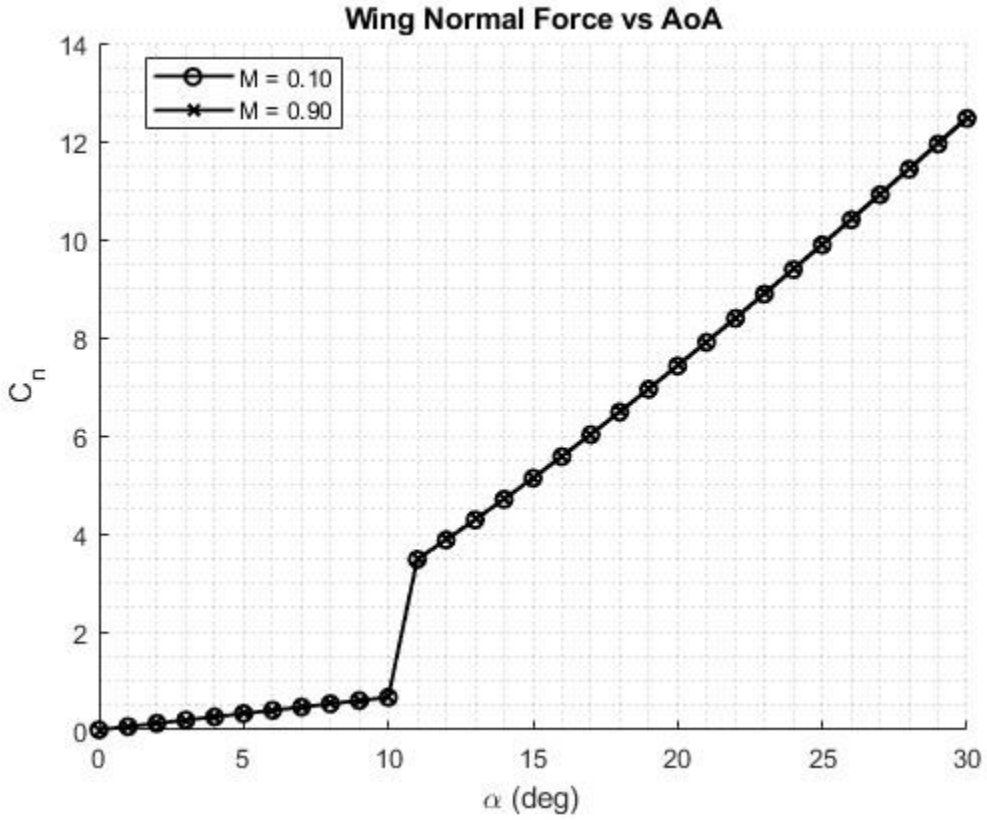

Figure 20 Wing Normal Force Vs. AOA

Figure 20 shows how the normal force coefficient for the wing varies with angle of attack up to 30°. The response remains linear up to about 10°, consistent with lifting surface theory, before minor nonlinear effects begin to appear at higher angles.

Tail

The contribution of the vee-tail to the equivalent normal force coefficients are described below.

$$\left(C_{N_\alpha,HT}\right)_{eq} = \left(C_{N_\alpha}\right)_T sin^2(\Phi)$$

Using the low aspect ratio equations for planar normal force, and applying the relationship above,

$$\left(C_{N_{\alpha},HT}\right)_{eq} = 1.132\,[1/rad]$$

The previous tail did not produce any normal force.

Total Lift

The total lift per angle of attack can then be found by adding them. The total normal force coefficients and the component contributions are shown below in Figure 21.

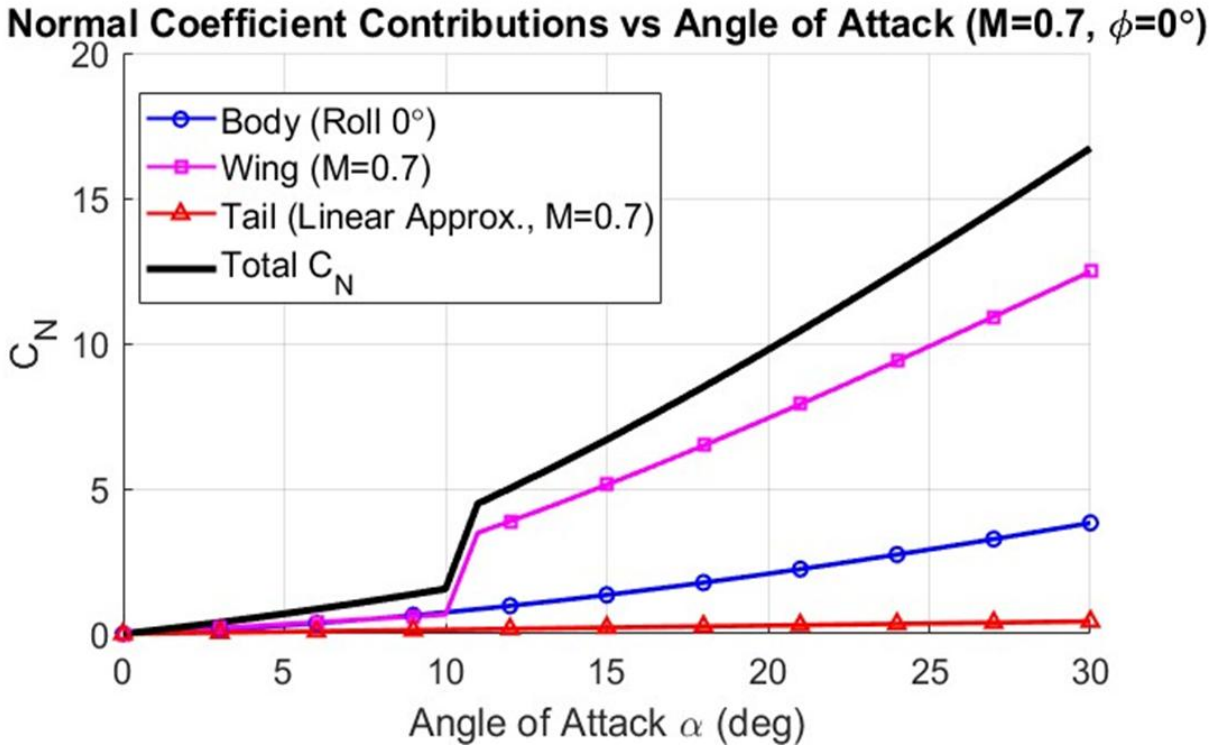

Figure 21 Total Lift per Angle of Attack

Figure 21 shows that the wing is clearly has the highest contribution in lift generated overall. The Body on the other hand does generate lift because of its flat surface on the bottom. However, the V-tail designed in WRAITH does not produce any lift.

O. Lift To Drag Performance

Table 5 Lift to Drag

Mach numbers	$\left(\frac{L}{D}\right)_{max}$
0.1	3.29
0.5	3.65
0.7	3.73
0.9	3.78

Zero-lift drag increase gradually as Mach increases, and no adverse aerodynamic behavior is observed. These results confirm stable aerodynamic drag performance for the redesigned missile within the Mach 0.1–0.9 flight envelope. From the table the highest L/D ratio is calculated at Mach 0.9.

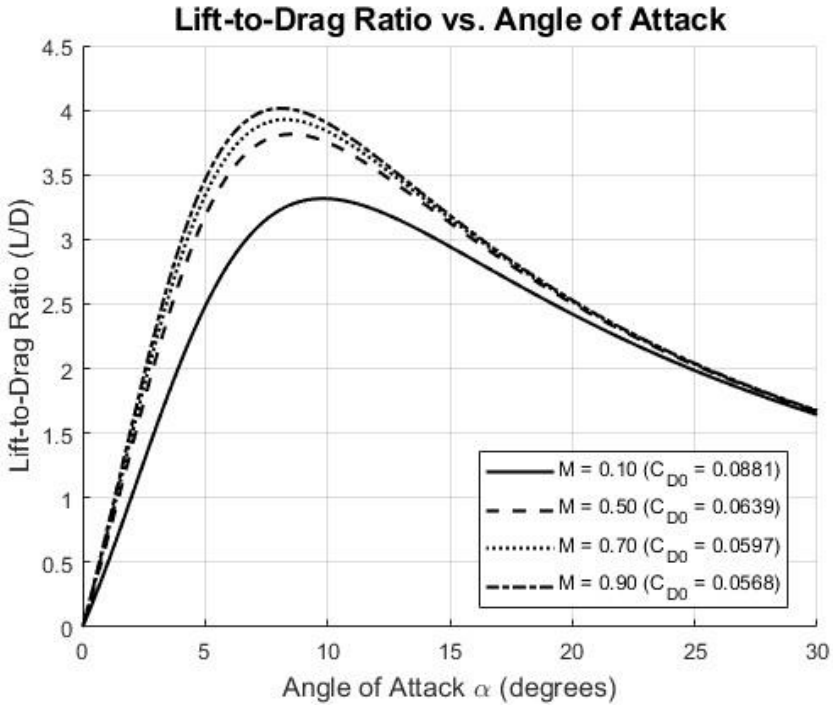

Figure 22 L/D over different Angles of Attack and Mach number

From graph 22, the body L/D ratio grows with an increase of AoA within the range of 0 - 10 deg. After this point, the drag increases more rapidly than lift, which results in a decline in the L/D ratio. This effect is explained mathematically by the following equation showing the increase in as the C_{D_n} increases.

$$\frac{L}{D} = \frac{C_L}{C_D} = \frac{(C_N \cos\alpha - C_{D_0} \sin\alpha)}{(C_N \sin\alpha + C_{D_n} \cos\alpha)}$$

P. Cruise

Cruise conditions:
Altitude: 2,000 ft
Mach Number: 0.71
Cruise AoA: $\alpha = 1.5°$

The cruise performance test for the missile was conducted to determine if the body and wing configuration can sustain a steady level flight at a lower altitude. In this analysis we chose a 2,000 feet altitude with a Mach number of 0.71 representing a subsonic long-range cruise. For this missile the design constraint is that at an $\alpha < 10$ The lift generated by the missile must equal the weight of the missile. Normal force coefficient and drag coefficient were calculated in previous sections and used here.

To calculate the lift coefficient both normal and drag coefficient were used in the following formula.

$$C_L(\alpha) = C_N(\alpha)cos\alpha - C_{D0,tot}sin\alpha$$

The dynamic pressure at 2,000 ft and Mach 0.7 is calculated in standard atmosphere and used to calculate the lift in the following equation.

$$L(\alpha) = C_L(\alpha)qS_{ref}$$

Table 6 cruise condition and results

Parameter	Values
Altitude	2,000 ft
Mach number	0.71
Weight (W)	1,975 lbf
Tail area (S_{tail})	3.36 ft^2
Wing area (S_{Wing}) Tail area (S_{Tail})	9 ft^2 3.64 ft^2
Cruise satisfied at α	1.5°

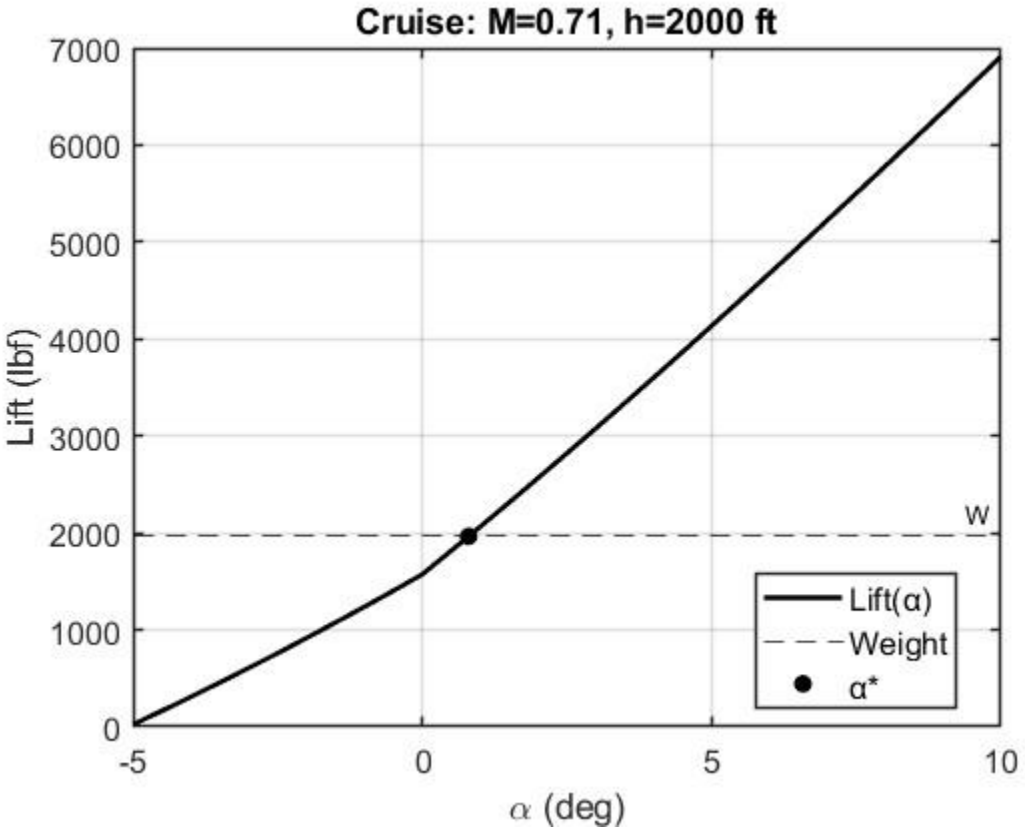

Figure 23 Cruise Lift per Angle of Attack

From Table 6 and graph 23 the missile body and wing surface satisfies the required cruise conditions at an angle of attack of $\alpha = 1.5°$ as that the missile will generate lift equal to the weight at that angle. Within $\alpha < 10°$ the maximum lift generated is almost 7,000 lbf indicating that the missile design has sufficiently generated lift.

The angle of attack at which the cruise is achieved shows that the chosen wing geometry is adequate for a Mach 0.71 cruise in a lower atmosphere. The fuselage does generate lift, but the

addition of lifting surface is required to reduce the α into a practical operating range. Figure 24 shows a free body diagram of WRATH in cruise conditions.

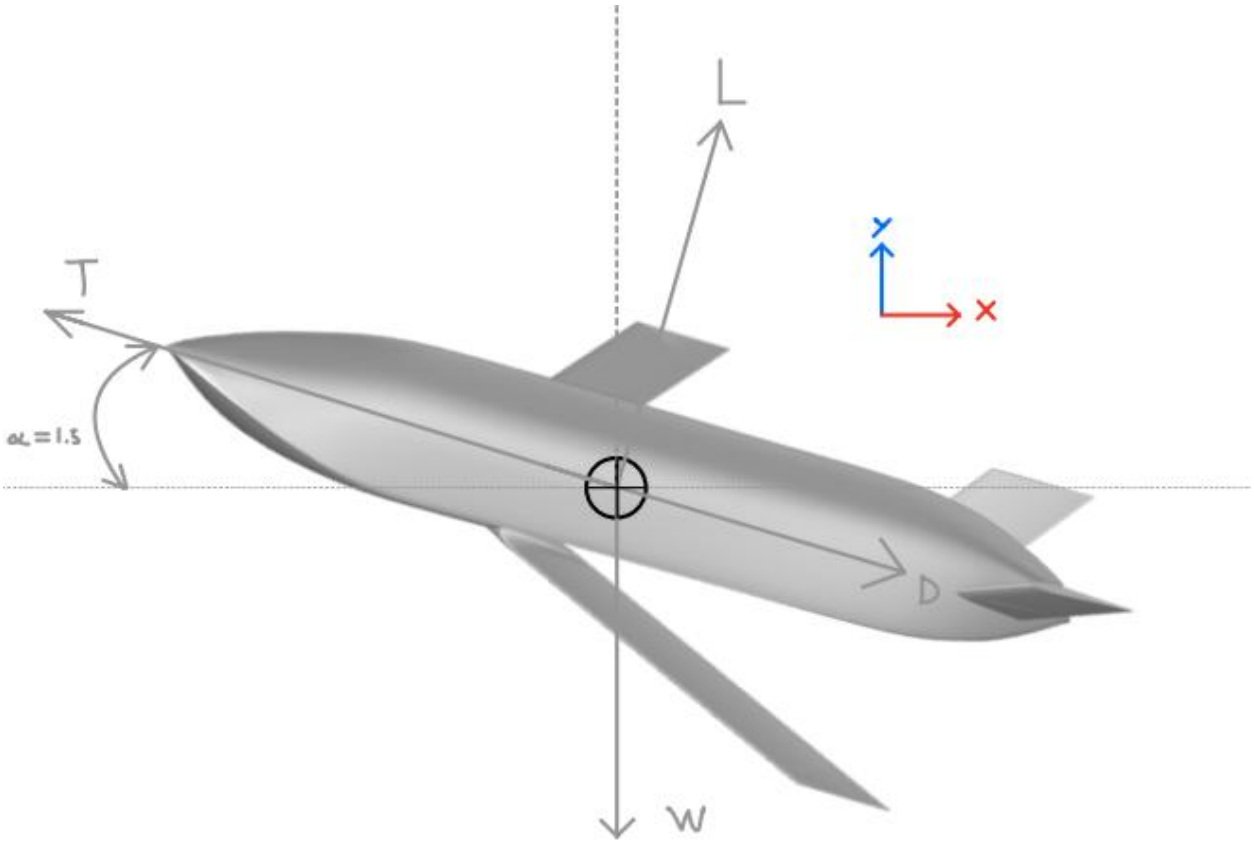

Figure 24 FBD of WRATH at Cruise

VI. Propulsion

Q. Design Constraints and Objectives

The redesign effort is bound by strict geometric and performance constraints. The propulsion system must fit within the existing missile body diameter of 21.61 inches. The engine is analyzed as an ideal turbojet with real component efficiencies applied to the compressor and combustor sizing. Finally, validation of the range capability using the new equation.

$$R = \left(\frac{L}{D}\right) I_{SP} V_{avg} \ln\left[\frac{W_E + \left(W_p - \dot{W}_p t\right)}{W_E}\right]$$

The baseline design of the compressor stages was comprised of three axial compressors. This yielded a maximum compression ratio of 7.61, which is under the given limit of 10. It is generally thought that increasing the pressure ratio to this maximum will allow for more efficient combustion, and thus a more powerful and efficient engine. By increasing the pressure ratio, the thrust for the given fuel rate can be maximized, so that the engine requires less fuel for the same thrust.

R. Compressor Angular Speeds

Using a maximum compressor diameter of 16 inches to allow for structure around the engine, the following diameters were found for each compressor, shown in Table 7

Table 7 Compressor Section Diameters

Axial Compressor 1 (C1) Diameter (ft)	1.0118
Axial Compressor 2 (C2) Diameter (ft)	1.1187
Centrifugal Compressor (C3) Diameter (ft)	1.3300

Using these diameters, the angular speeds and pressure ratios (PR) for each section can be found as well as the total pressure ratio. These speeds and pressure ratios are shown in Table 8. It is seen that as the initial temperature increases, it is more difficult for the axial compressors to function, so the centrifugal compressor must pick up the lost compression. Through this design, the pressure ratio of 10 was essentially achieved, and the angular speeds and pressure ratios should be noted as a maximum for the engine.

Table 8 Pressure Ratios and Rotation Speed

T2 (°R)	N (rpm)	PR_{C1} (~)	PR_{C2} (-)	PR_{C3} (-)	PR_{Tot} (-)
441.49	18667	1.8522	1.8853	2.8619	9.9934
505.62	19886	1.8424	1.8795	2.8863	9.995
563.11	20905	1.8342	1.8746	2.9068	9.9946
544.55	20583	1.8369	1.8761	2.9004	9.9952
602.65	21574	1.8291	1.8715	2.9213	9.9997

Table 9 shows the temperature after each section. Note that C2.6 is the station after C2.

Table 9 Compressor Temperature

T_2 (°R)	$T_{2.3}$ (°R)	$T_{2.6}$ (°R)	T_3 (°R)
441.49	526.62	629.76	847.23
505.62	601.14	716.84	963.46
563.11	667.65	794.23	1066.5

544.55	646.2	769.3	1033.4
602.65	713.26	847.18	1137.1

S. Fuel-to-Air Ratios

To maintain the required turbine inlet temperature (T_4) of 4000 °R, the fuel-to-air ratio is adjusted based on the compressor exit temperature (T_3). Based on the temperatures in Table 10, the required fuel-to-air ratio ranges from approximately 0.046 at low altitude (10 ft) to 0.052 at high altitude (30,000 ft).

Table 10 MATLAB Output for Compressor Outlet Temperature

Altitude (ft)	Tt2 (R)	Compressor Outlet Temperature (Tt3) in R
10	602.7	1,137
2,000	544.6	1,033
3,000	563.1	1,067
15,000	501.27	963
30,000	441.49	847

Figure 6 illustrates the fuel-to-air ratio required to heat the compressed air to the target turbine inlet temperature (T_4) of 4000 °R. As shown in Table 10, the compressor outlet temperature (T_3) varies significantly during flight, from a high of 1,137 °R at sea level to a low of 847 °R at 30,000 ft.

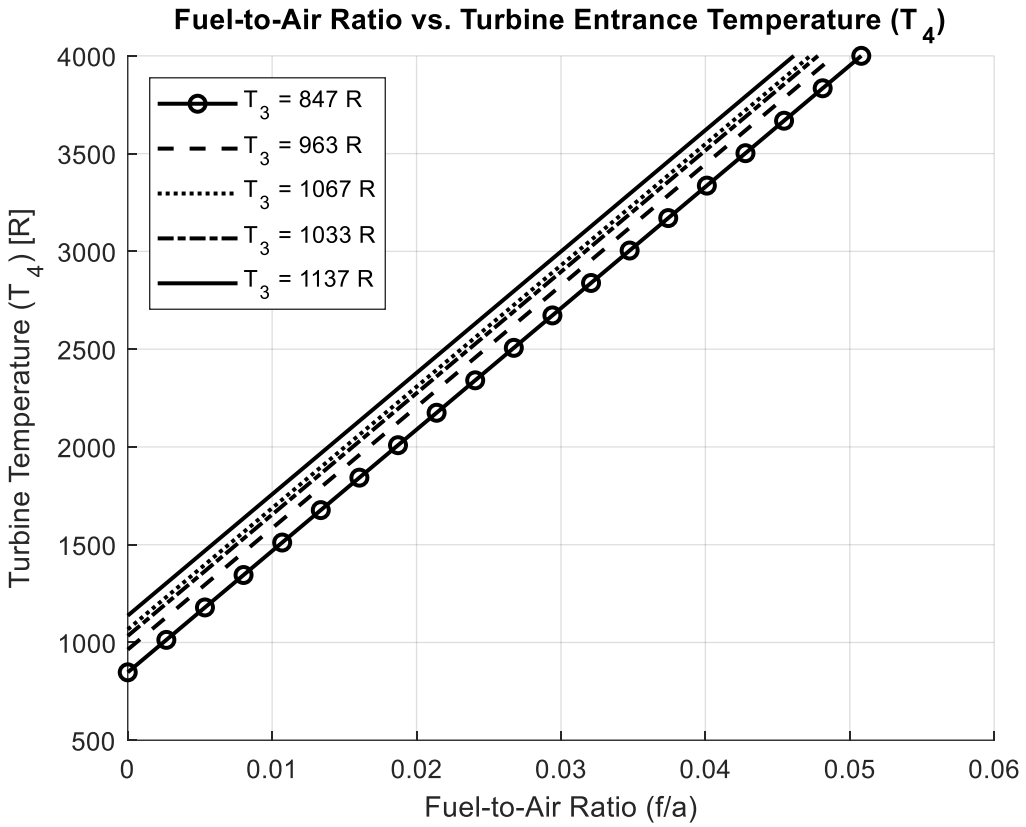

Figure 25 Fuel-to-air Ratio vs T4

Consequently, the required fuel-to-air ratio fluctuates to maintain constant thrust performance. According to the data presented in Figure 25, the operational ratio ranges from approximately 0.046 at sea level (to heat the hotter air) up to 0.052 at altitude (to heat the colder air). For the purpose of the conservative range calculation, a baseline limit of 0.04 was utilized to ensure structural margins were maintained.

Figure 26 shows the thrust increases as Mach number increasing for different operational altitudes. The performance curves for the WRAITH turbojet engine demonstrate the primary trends within the subsonic flight envelope in Figure 26. The thrust increases with Mach number at all chosen altitudes. Additionally, as pressure and temperature decrease, thrust also decreases. The most thrust of almost 1600 lbf are created when closing in the target at 10ft

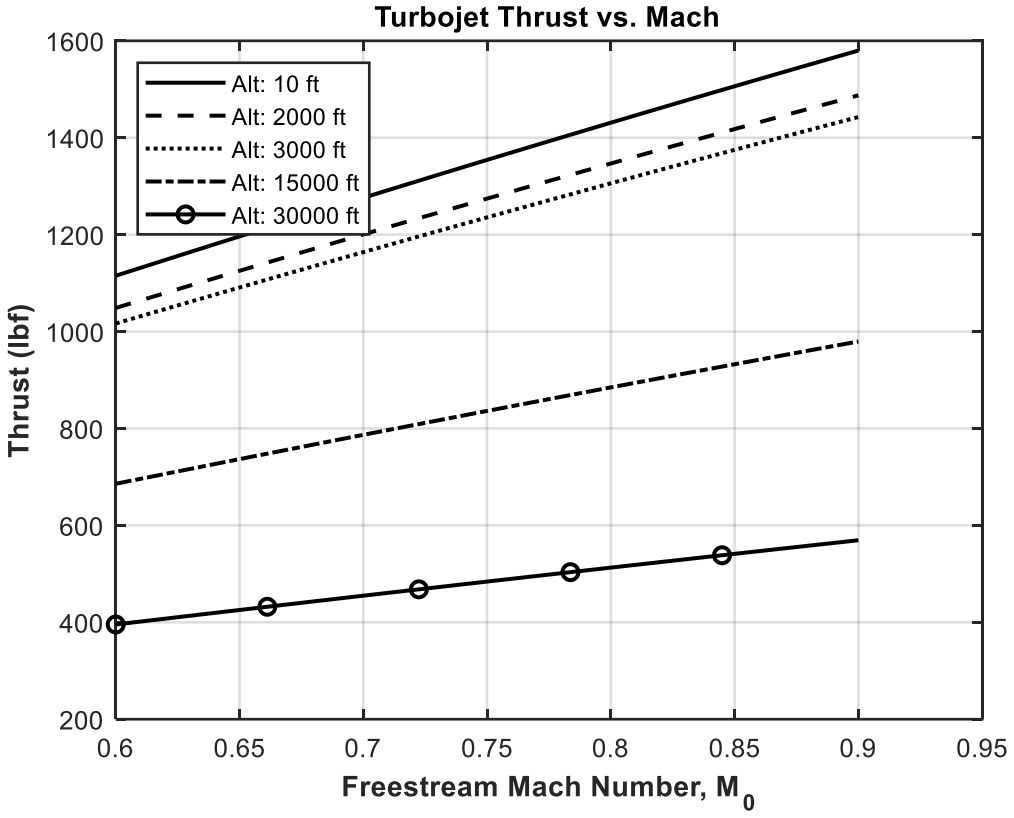

Figure 26 Thrust at different Mach Number

To achieve the required thrust levels across the flight envelope, the engine controller must modulate the fuel-to-air ratio to maintain a constant turbine inlet temperature of 4000 Rankins. Our simulation indicates that the required fuel-to-air ratio ranges from a minimum of 0.046 at Sea Level (10 ft) to a maximum of 0.052 at the operational ceiling (30,000 ft)

This variation is thermodynamically driven by the changes in compressor outlet temperature. At low altitudes, the ambient air is denser and warmer, resulting in a higher T_3 at 10 ft). Additionally, less fuel is required to raise the air temperature to 4000 Rankins. Moreover, at high altitudes (30,000 ft), the inlet air is significantly colder, resulting in a lower T_3, which necessitates a higher fuel-to-air ratio to bridge the larger temperature gap and achieve maximum thrust efficiency.

While the operational ratio peaks at 0.052, a conservative baseline of 0.04 was utilized for the flight range and fuel weight calculations to ensure structural margins were maintained and to account for non-ideal combustion inefficiencies.

T. Specific Impulse

Specific impulse quantifies the efficiency of the propulsion system by normalizing thrust against the weight flow rate of the fuel. For this design, I_{sp} was calculated analytically using the thermodynamic relationship shown in equation below, which accounts for the engine's maximum temperature ratio and the designed compressor pressure ratio of 10.

$$\left[g_0 c_p T_0/\left(a_0 H_f\right)\right](I_{SP})_{Tmax} = T_{max}/(p_0 A_0)/\left[\gamma_0 M_0\left[(T_4/T_0) - (p_3/p_2)^{(\gamma_0-1)/\gamma_0}\right]\right]$$

Figure 27 illustrates the variation of specific impulse across the flight envelope. Throughout the simulated mission profile, the specific impulse ranges from a minimum of approximately 2,830 seconds at high subsonic speeds (Mach 0.9) to a maximum of 2,930 seconds at cruising conditions.

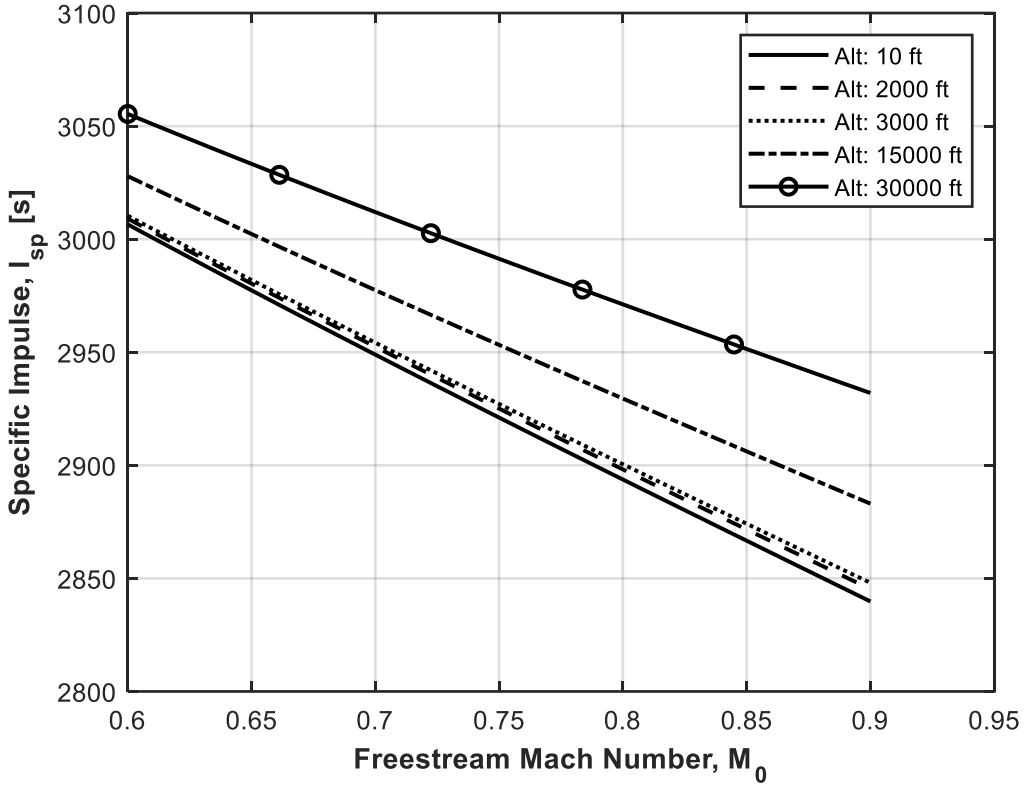

Figure 27 Specific Impulse

U. Remaining Range

To evaluate the operational endurance of the WRAITH redesign, the remaining flight range was calculated using the modified Breguet range equation for turbojet propulsion, as shown below

$$R = \left(\frac{L}{D}\right) I_{SP} V_{avg} \ln\left[\frac{W_E + \left(W_p - \dot{W}_p t\right)}{W_E}\right]$$

where W_E represents the empty weight and W_p represents the fuel weight. The analysis utilized a cruise Lift-to-Drag ratio of 3.93, derived from the aerodynamic performance at the average cruise velocity. The fuel mass flow rate was calculated to be 0.016 lbs/s based on the previously determined fuel-to-air ratio of 0.04 and an air mass flow rate of 0.35 lbs/s.

Figure 28 presents the remaining range profile over the duration of the powered flight. The plot exhibits a linear decay in remaining range, corresponding to the steady depletion of fuel at a constant cruise velocity. As the burn time progresses, the missile weight decreases slightly, which improves efficiency with the consumption of 350 lb fuel load.

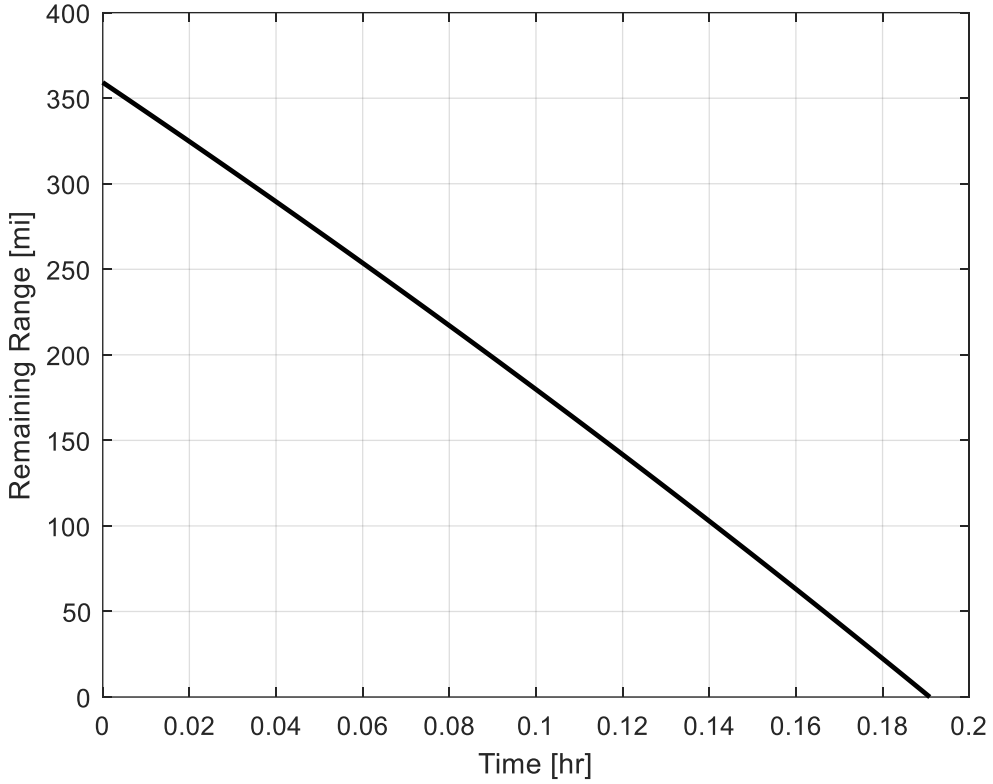

Figure 28 Remaining Range

The simulation indicates a maximum flight endurance of 11.4 minutes. This corresponds to a total powered range of 360 miles or 313 nautical miles. This performance represents a 40% increase over the baseline design range of 250 miles or 217 nautical miles, successfully achieving the threshold requirement for redesigning effort.

VII. Missile Trajectory

The missile follows a multi-phase trajectory beginning with a high-altitude release from a B-2 platform at approximately 40,000 ft ASL, after which it stabilizes and immediately enters a commanded steep dive to rapidly descend out of the high-altitude environment. This dive minimizes exposure to long-range surveillance radars and converts potential energy into kinetic energy, allowing the missile to accelerate efficiently without excessive fuel use. As it approaches the designated operating altitude, the missile performs a controlled flare maneuver to gradually reduce its dive angle, arrest its descent, and limit structural loading while transitioning into low-altitude cruise. Once established below 2,000 ft AGL, the missile flies a sustained terrain-masked cruise segment, using low altitude, small lateral corrections, and altitude adjustments to reduce radar line-of-sight and avoid known radar coverage. Upon entering the terminal area, the missile commands a shallow pitch-up to position itself for a low-angle glide, trading a small amount of energy for improved accuracy and control authority. The trajectory concludes with a low-observable, shallow terminal glide toward the stationary target, maintaining minimal radar exposure until impact. Figure 29 shows the planned trajectory of the WRAITH, the trajectory is intentionally shortened to better illustrate the flight phases.

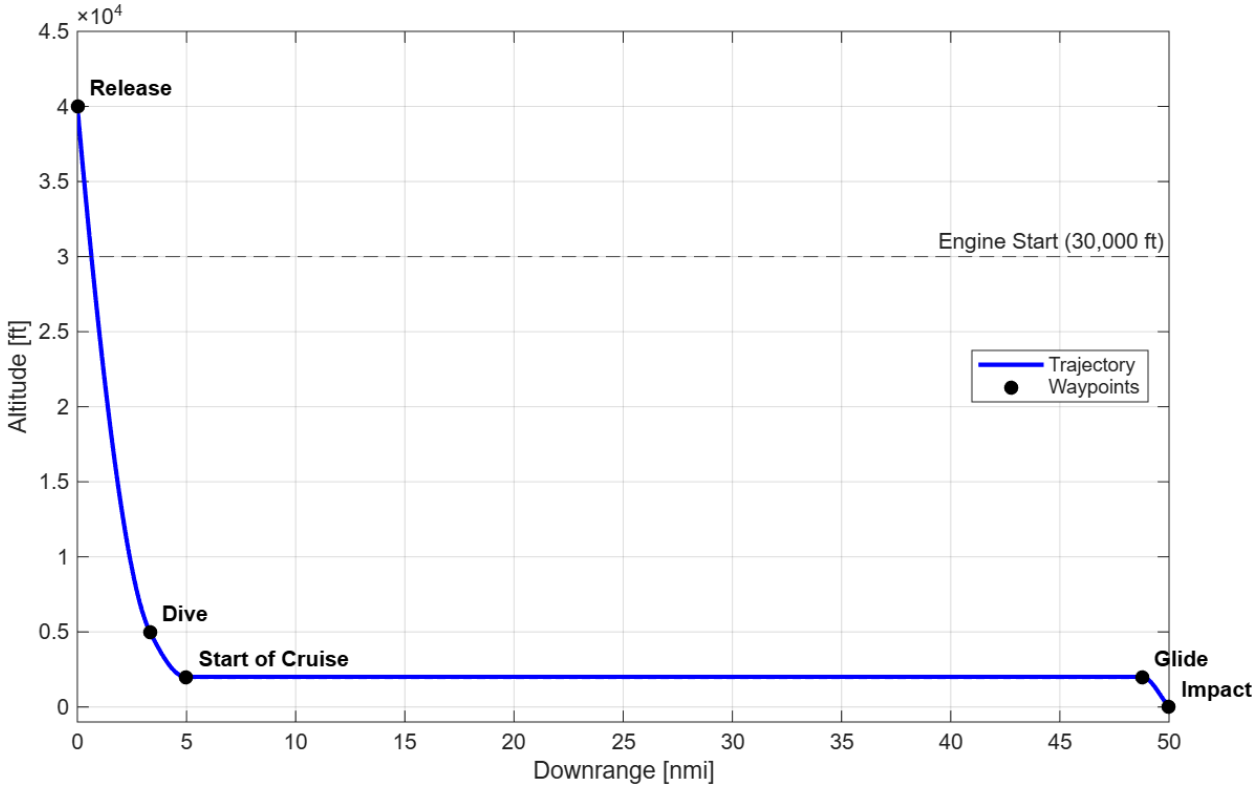

Figure 29 WRAITH Trajectory

A. Missile Release and Dive

Following the release from the B-2 platform at approximately 40,000 ft ASL, the missile enters a controlled separation phase to ensure clean aerodynamic and inertial decoupling from the aircraft.

Immediately after release the wings and tail deploy, and the missile enters a controlled dive to rapidly decrease in altitude. The dive is intentionally commanded to a steep dive angle to minimize exposure to long-range radar and to convert the missiles potential energy into kinetic energy without significant fuel usage.

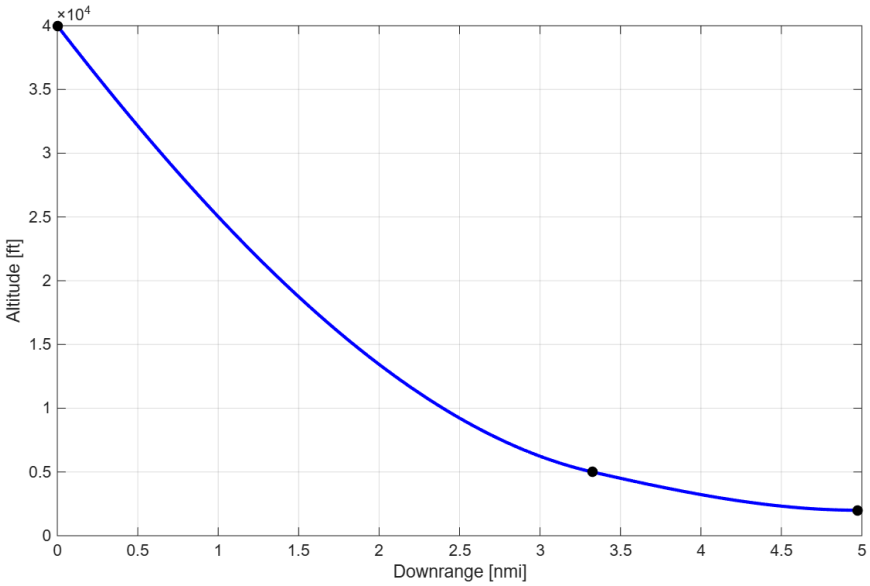

Figure 30 Dive Trajectory

B. Low-Altitude Cruise and Radar Avoidance Behavior

Once the missile has reached the low-altitude segment of the flight, the missile enters its terrain-following and radar-avoidance phase. Flying at low-altitude reduces the detectability to ground-based radar by using terrain features for natural masking, reducing the radar horizon range, and limiting exposure to long-range search radars. During cruise the missile performs both lateral maneuvers to follow the desired trajectory and longitudinal corrections to maintain a low ground clearance.

Using stored elevation maps of the target range, and on missile measured altitude, the WRAITH uses a Terrain Contour Matching (TERCOM) [11] concept to stay at low altitude. Figure 31 shows the basic process of the concept. Using a pre-collected terrain map of the range, the missile can then maintain a desired altitude above the ground. Measurements taken from the missile then update the missile position compared to the terrain data and inform the missile of its current position and the altitude maneuvers needed to maintain the desired height.

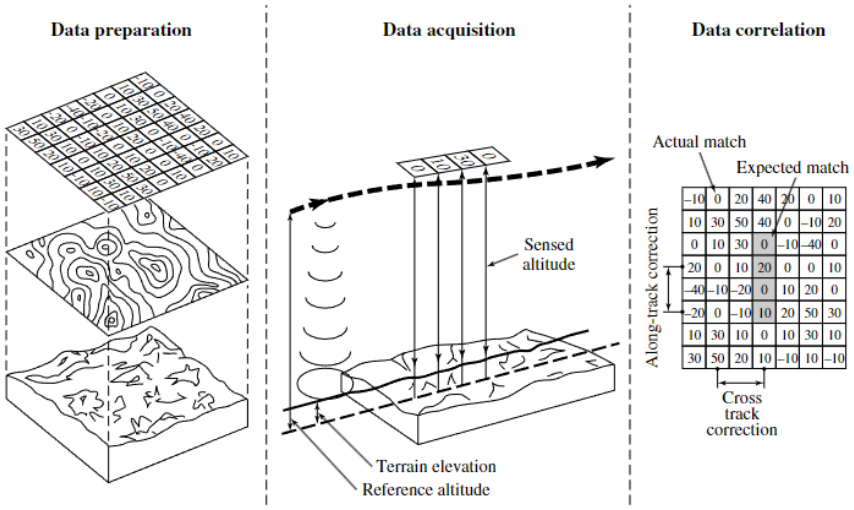

Fig. 7.11. *TERCOM* concept.

Figure 31 Overview of TERCOM Concept [11]

Figure 32 below shows an example terrain map and trajectory to avoid radar sites. The path is determined by maintaining a low altitude and remaining as far away from the radar sites as possible. In addition to terrain, the map also includes the locations of radar threat sites. The trajectory shown in Figure 32 reflects a combined objective: maintain low altitude to reduce detection probability and shape the lateral path to maximize separation from radar coverage zones. In this sense, TERCOM enables the missile to confidently execute aggressive low-altitude routing because its position relative to the underlying terrain can be continuously verified against the pre-stored map.

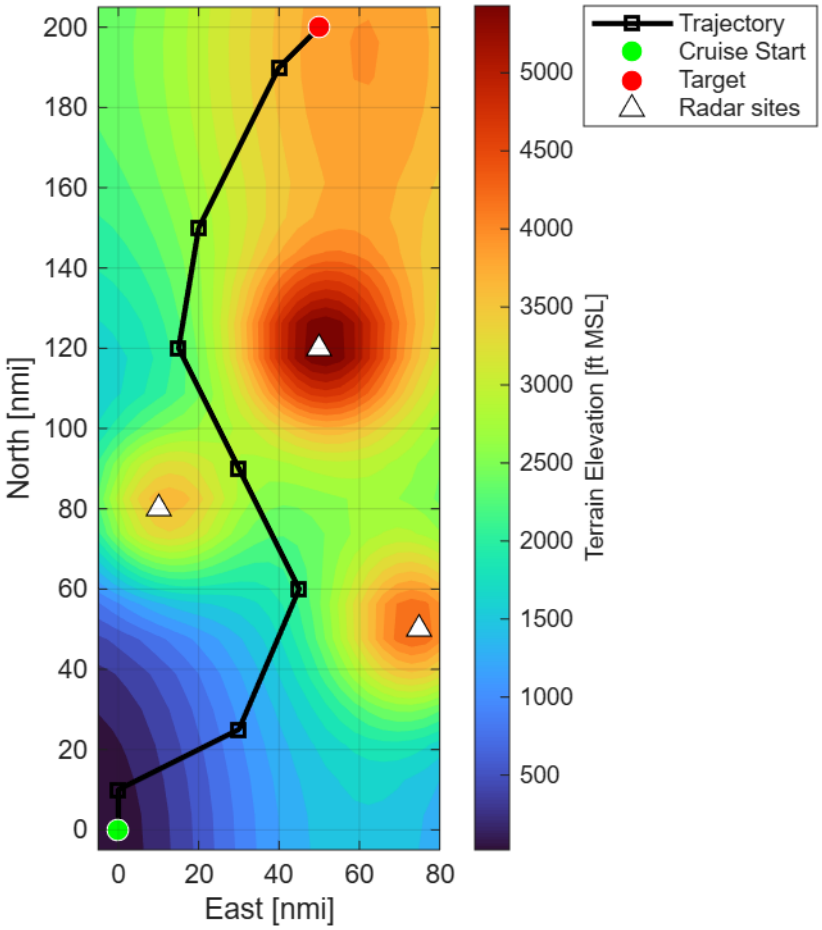

Figure 32 2D Terrain Map and Trajectory

During mission planning, this terrain-based approach determines where the missile can safely descend, where it must climb slightly to clear terrain features, and how far it must offset from radar sites to stay outside their effective detection ranges. The result is a trajectory that remains terrain-hugging over most of the route, takes advantage of natural terrain masking, and threads the missile through regions where radar line-of-sight is minimized.

Overall, the 2-D terrain map provides the structural foundation for defining a viable low-altitude, radar-avoiding trajectory. The terrain-based guidance approach ensures the missile can remain on this planned path throughout the midcourse phase, enabling the flight profile shown in Figure 16 to reliably guide the missile toward the target while minimizing exposure to detection.

Figure 33 shows the same map projected in 3D space, the trajectory ensures that WRAITH stays a constant distance above the ground throughout the cruise phase.

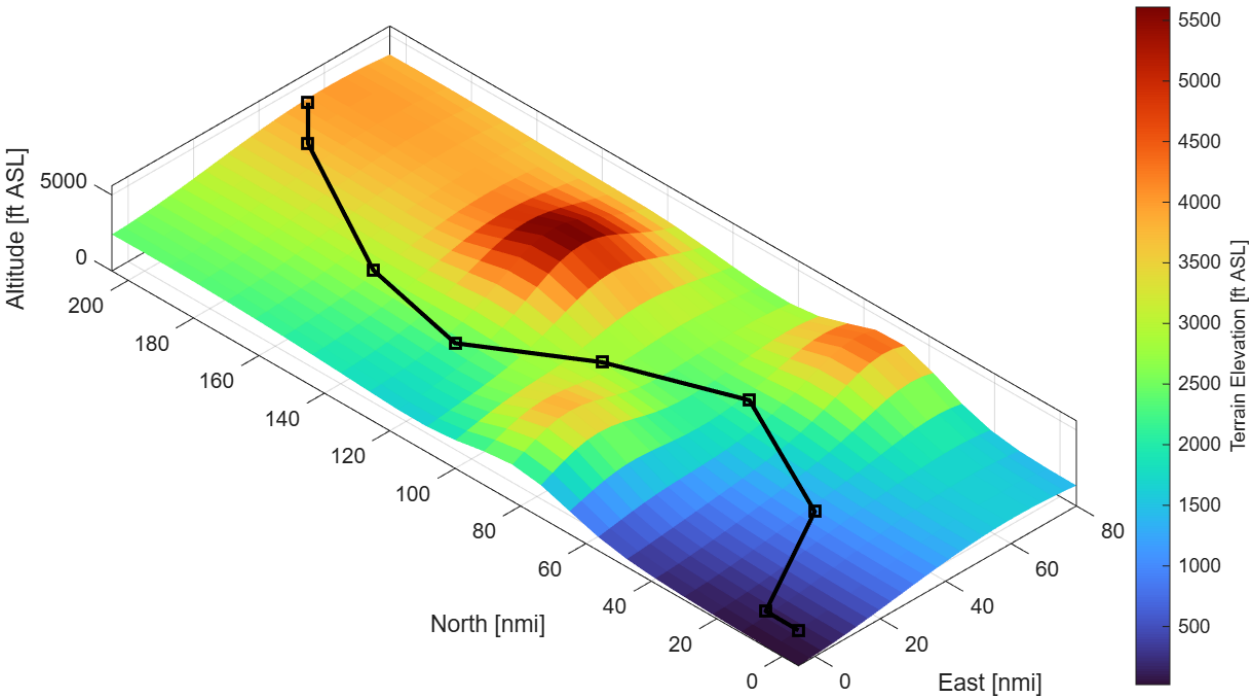

Figure 33 3D Terrain Map and Trajectory

C. Terminal Maneuvering

Once this missile reaches the chosen engagement distance from the desired target, the WRAITH shifts from and low-altitude cruise to a controlled low-angle glide while maintaining low observability. The maneuver gives WRAITH a stable tracking environment without exposing the missile to increased exposure. The goal of this phase is to prioritize precision, using small corrections to maintain the desired heading and glide angle. The figure below shows a zoomed in view of the 2D glide to impact trajectory.

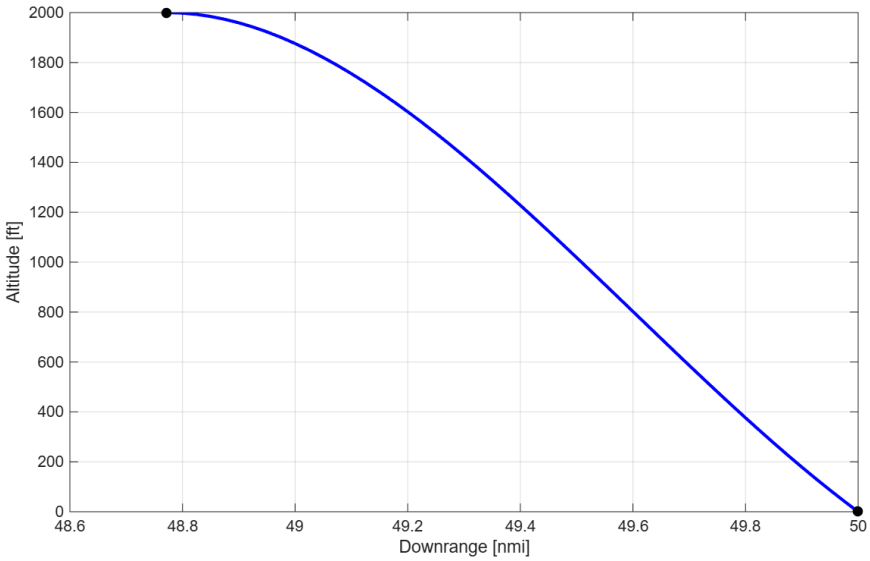

Figure 34 Glide Trajectory

VIII.Trajectory Simulation

A. Equations of Motion

The translational equations of motion are defined below. Force (F) is defined as the derivative of momentum (p).

$$P = mV$$
$$\sum F = \frac{d}{dt}P$$

Calculating the derivative of p in respect to time and accounting for changing mass, the following terms are derived using the product rule. Shown in the equation below.

$$\sum F = \frac{d}{dt}(mV) = m\frac{dV}{dt} + \frac{dm}{dt}V = ma + \dot{m}V$$

The ma term captures the standard equation of motion, while the $\dot{m}V$ term capture the mass ejection in respect to the body coordinate system

Like the translational equation of motion, the rectangular equations of motion are defined using the angular momentum (H), where the angular momentum is defined by the total moment in the body.

$$H = \int r \times (\omega \times r) dm = mr \times (\omega \times r)$$

Simplifying the equation to isolate pitching moment, the angular momentum becomes:

$$H_y = Q \int (z^2 + x^2)\, dm = QI_y$$

Taking the derivative of the angular momentum and applying the product rule, the total pitching moment is defined using the equations below.

$$\sum M = \frac{d}{dt}H_y$$
$$\sum M = \frac{d}{dt}(QI_y) = Q\frac{dI_y}{dt} + \frac{dQ}{dt}I_y = Q\dot{I_y} + \dot{Q}I_y$$

This derivation captures both how the change in pitching angular acceleration and the change in moment of inertia changes the pitching dynamics of the missile. Due to the changing mass of the missile effecting both the rectilinear and angular acceleration of the missile, it will be important to consider when constructing a simulation of the WRAITH.

A two-dimensional (2-D) missile flight simulation was developed in Simulink to model motion in the horizontal direction X and vertical direction Z. The simulation propagates the nonlinear equations of motion using time-stepped aerodynamic, propulsion, and gravitational forces. The objective of this model is to generate a complete flyout profile that demonstrates the missile's ability to perform its required dive, flare, low-altitude cruise, and terminal glide segments as specified in the CONOP.

Unlike a coefficient-based aerodynamics approach using $C_L$and C_D, the aerodynamic model used in this simulation produces body-axis forces directly in terms of normal force $N$and axial force A. Both $N(\alpha, M)$and $A(\alpha, M)$are obtained from the previously developed aerodynamic database, which tabulates force predictions as functions of angle of attack $\alpha$and Mach number M. At each time step, the simulation updates $\alpha$and M, queries the aerodynamic tables, and applies the resulting body-axis forces immediately to the equations of motion.

The primary translational dynamics are formulated in the missile body frame. The total force along the body X axis is

$$F_X = T + A - W\sin(\theta),$$

where T is thrust and W is weight. The total force along the body Z axis is

$$F_Z = W\,cos(\theta) - N.$$

This set of equations matches the free-body diagram of the missile with the total forces applied to the body.

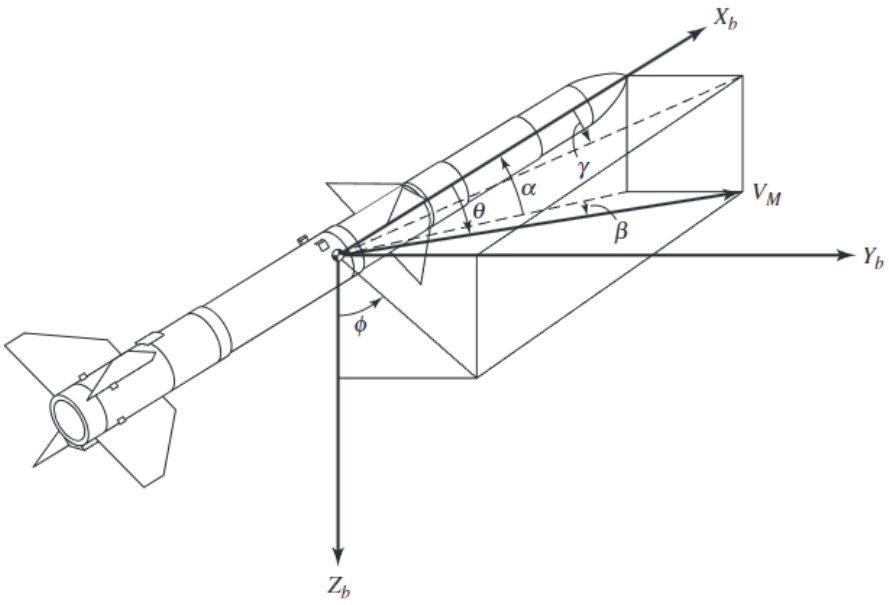

Fig. 3.5. Missile angular relationships.

Figure 35 Missile Angular Relationships [11]

Because the simulation uses the inertial frame, these body axis forces are converted to the inertial reference frame using the following set of equations:

$$F_{X_I} = F_{X_B}\, cos(\theta) - F_{Z_B}\, sin(\theta)$$
$$F_{Z_I} = F_{X_B}\, sin(\theta) + F_{Z_B}\, cos(\theta)$$

The rotated forces can then be used to find the acceleration of the missile in inertial coordinates.

Because the angle of attack is a measured output and not an independent input, the command input must be the control surface deflection. For our missile, the ruddervators serve a dual function, the missile can be pitched using the elevator function to balance the aircraft.

$$C_N = \left(C_{N_\alpha}\right)_B \alpha + \left(C_{N_\alpha}\right)_W \alpha + \left(C_{N_\delta}\right)_B \delta$$

$$C_M = \left(C_{M_\alpha}\right)_B \alpha + \left(C_{M_\alpha}\right)_W \alpha + \left(C_{M_\delta}\right)_B \delta$$

The complete model is stepped forward in time from the release to the target impact, producing a continuous 2D trajectory. This allows for full verification that the aircraft can meet the maneuvering requirements of the trajectory.

B. Simulation Setup

Two simulations were made for the model, one for the launch/high-degree dive and another for the terminal/low-degree dive.

The high-degree dive was set with an initial velocity of 800 ft/s with a 60-degree dive angle starting at 40,000 ft. The engine starts at 30,000 ft and ramps up through the dive. Figure 36 shows the missile velocity in body coordinates through the dive.

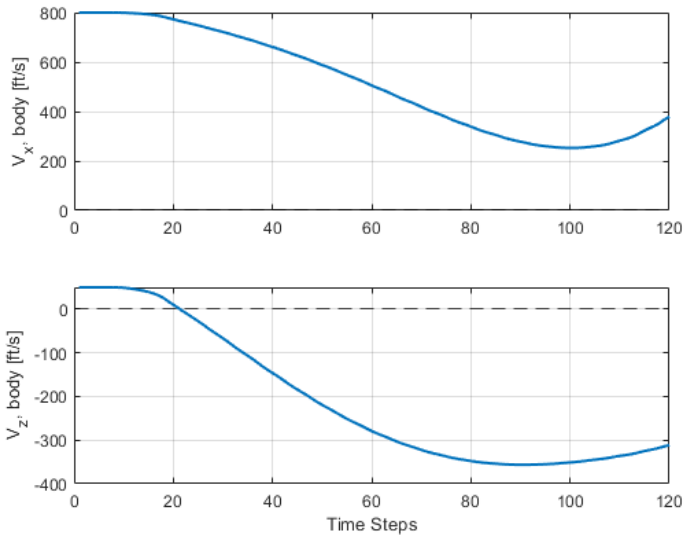

Figure 36 High-Angle Dive Missile Body Velocities

The forward velocity (V_x) initially decreases due to drag, while the vertical velocity (V_z) increases in magnitude with the acceleration due to gravity. As the engine turns on and ramps up, the forward velocity slowly increases as the missile transitions to level flight. The missile remains at a high angle of attack through the maneuver to follow the desired flare path. Figure 37 shows the resulting trajectory from the initial conditions. The trajectory shows a steep dive followed by a smooth transition to level flight.

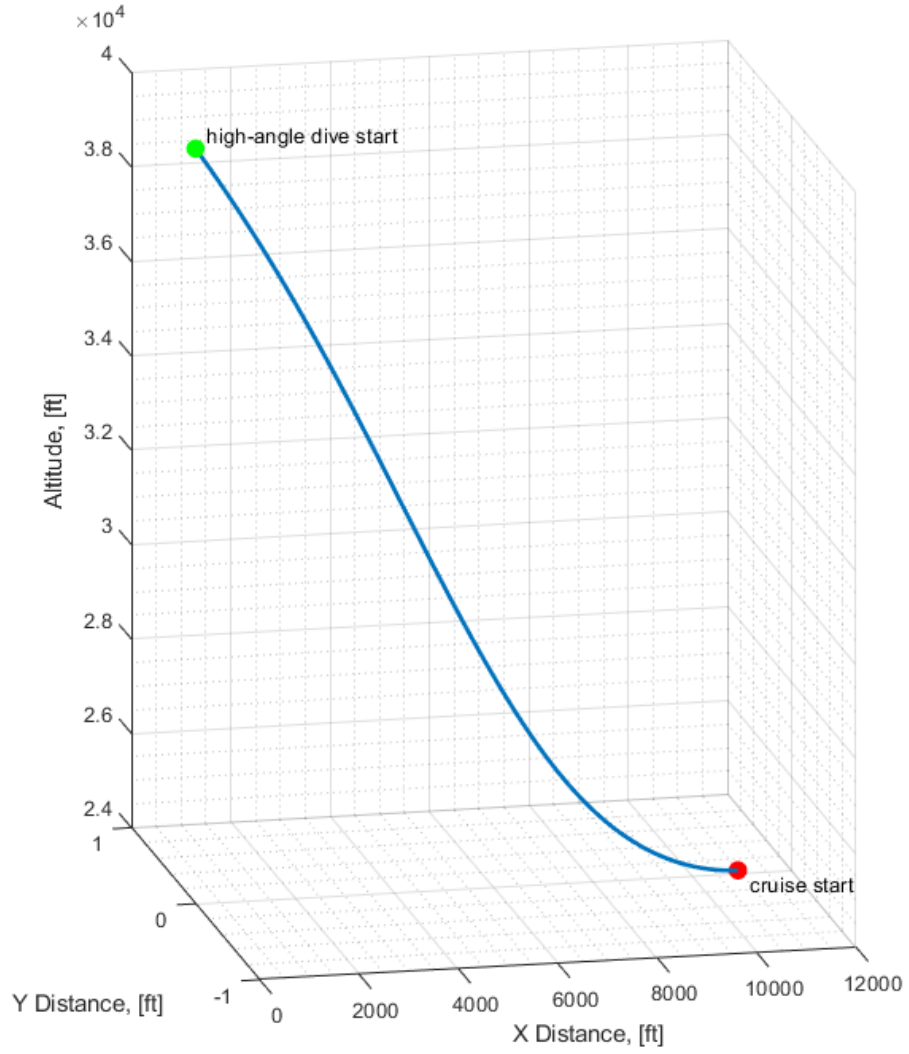

Figure 37 High-Degree Dive from 40,000 ft

The low angle dive starts with a velocity of 800 ft/s at an altitude of 2,000 ft. The dive angle is initially set at 5 degrees. The low-angle dive body velocities are shown in Figure 38. The forward velocity gradually increases, while the vertical velocity sharply flips signs, indicating the transition to dive.

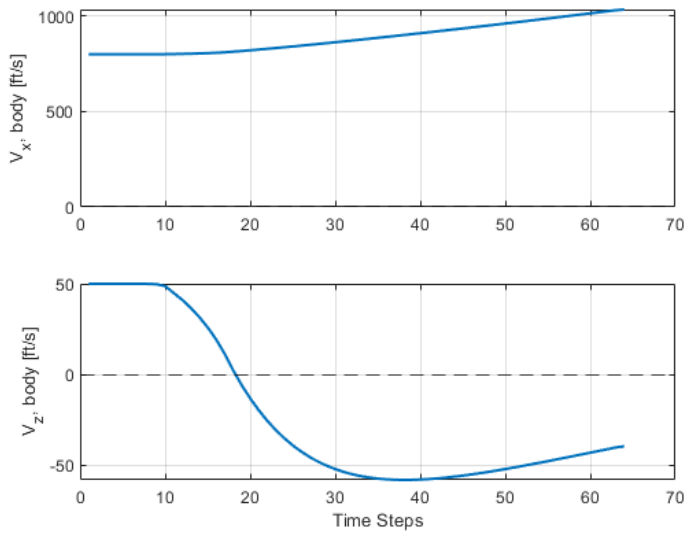

Figure 38 Low-Angle Dive Missile Body Velocities

Figure 39 shows the trajectory of the low-angle dive. The graph shows a smooth transition from cruise to impact with the ground. The simulations show that the chosen trajectory is achievable with the current design.

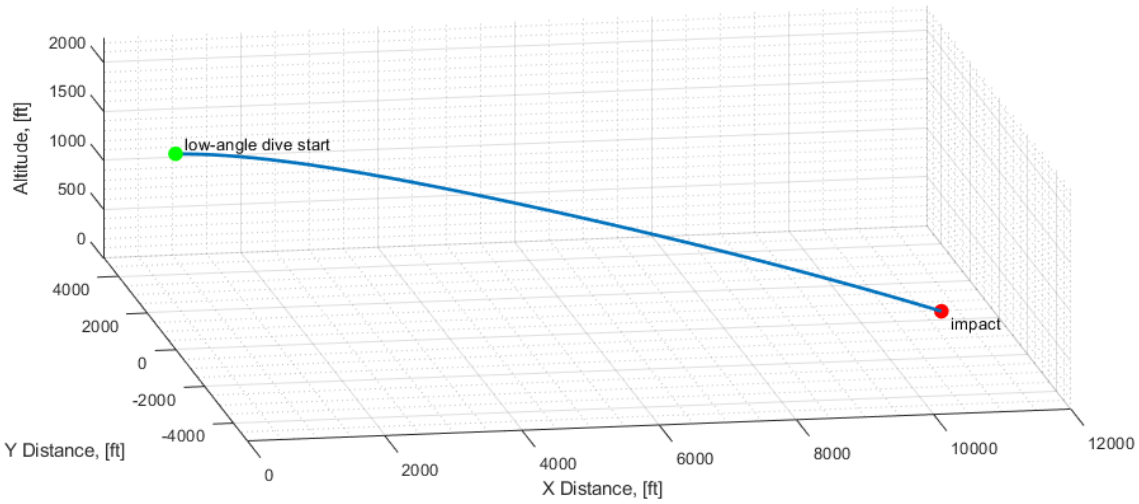

Figure 39 Low-Angle Dive From 2,000 ft

IX.References

[1] Svitlyk, Y. "AGM-158 JASSM: Joint Air-to-Surface Standoff Missile." Root Nation, November 25, 2024. https://root-nation.com/en/articles-en/weapons-en/en-agm-158-JASSM-air-launched-cruise-missile/

[2] Siemens Digital Industries Software, *NX* [computer software], Version 2306, Siemens Digital Industries Software, Plano, TX, 2023. URL: https://www.plm.automation.siemens.com/global/en/products/nx/

[3] Airforce Technology, "AGM-158 JASSM (Joint Air-to-Surface Standoff Missile)," Airforce Technology Projects, July 5, 2013. Available: https://www.airforce-technology.com/projects/agm-158-jassm-standoff-missile/

[4] USAF launches JASSM New Variant Missile. Default. (n.d.). https://www.janes.com/osint-insights/defence-news/weapons/usaf-launches-JASSM-new-variant-missile

[5] UPDATED JASSM® completes important Lockheed martin flight tests. Media - Lockheed Martin. (n.d.). https://news.lockheedmartin.com/2017-03-08-Updated-JASSM-R-Completes-Important-Lockheed-Martin-Flight-Tests

[6] U.S. Standard Atmosphere, 1976, NOAA-S/T-76-1562, NASA-TM-X-74335, National Oceanic and Atmospheric Administration, Washington, D.C., Oct. 1976. Available: https://www.robertribando.com/xls/fluid-mechanics/1976-u-s-standard-atmosphere/

[7] Fleeman, E. L., & Schetz, J. A. (2012). *Missile Design and System Engineering*. American Institute of Aeronautics and Astronautics.

[8] OpenVSP, *Open Vehicle Sketch Pad (OpenVSP), Version 3.33.0*, NASA Open Source Software, 2025. Available: https://openvsp.org

[9] Drela, M. Flight Vehicle Aerodynamics. Cambridge, MA: MIT Press, 2014.

[10] The MathWorks Inc., *MATLAB, Version 9.15.0 (R2024b)*, Natick, MA, 2024. Available: https://www.mathworks.com

[11] G. M. Siouris, *Missile Guidance and Control Systems*. New York: Springer, 2003.

Phan, T., Hollman, N., Sievers, T., and Almazrouei, M., "Joint Air-to-Surface Standoff Missile," Dept. of Aerospace Engineering, University of Kansas, Lawrence, KS, 2025.

X. Appendix A

Weight – Nathaniel Hollman
Aerodynamics – Mohammed Almazrouei
Propulsion – Tri Phan
Missile Trajectory & Trajectory Simulation – Tiger Sievers